Mechanical Systems and Signal Processing 174 (2022) 109042

Contents lists available at ScienceDirect

Mechanical Systems and Signal Processing

journal homepage: www.elsevier.com/locate/ymssp

Damping parameter estimation using topological signal processing

Audun D. Myers *, Firas A. Khasawneh

Department of Mechanical Engineering, Michigan State University, United States of America

ARTICLE INFO

Communicated by L. Jankowski

Keywords:
Damping
Parameter estimation
Topological signal processing
Sublevel set persistence
Decrement

ABSTRACT

Energy is dissipated in engineering systems through a variety of different, typically complex, damping mechanisms. While there are several common damping models with physical interpretations, it is often necessary to examine noisy, experimental data in order to identify and fit the damping parameters. One class of methods fits the damping parameters based on the decay envelope of the signal's peaks based on some assumed damping mechanism. While there exist results in the literature, especially for viscous damping, to guide the selection of the spacing between the peaks for the optimum damping ratio identification, these methods often overlook the difficult and classic problem of identifying the signal's "true" peaks in the presence of noise. Therefore, in this work we utilize tools from Topological Data Analysis (TDA) to address the problem of robust and automatic power-law damping identification from decay or free-response function. The decay function can be obtained from initial excitation, or using random decrement method thus making our approach a viable tool for operational modal analysis. We present our approach using one-dimensional examples, and describe extensions to multiple degree of freedom systems. Our damping identification framework uses the persistent homology of zero dimensional (0D) sub-level sets, one of the main tools of TDA, to separate the true topological features of the signal (i.e. the peaks and valleys) from measurement noise. Using persistent homology we are able to automatically represent the damped response in a noise-robust, two-dimensional summary of the peak–valley pairs called the persistence diagram. The persistence diagram is then analyzed using two methods: (1) a theoretical analysis of the significant persistence pairs and (2) function fitting to the persistence space. We present theoretical results that establish the class of general power-law damping terms where our approach applies, and develop specific tools to identify damping parameters for viscous, coulomb, and quadratic damping. We show that our approach is computationally fast, operates on the raw signal itself without requiring any pre-processing, and reduces the number of decisions needed by the user to perform the needed calculations. The results are validated using a combination of numerical and experimental data.

1. Introduction

Damping mechanisms play an important role in many real-world applications including structural health monitoring [1], dynamics of robotic systems [2,3], power systems [4,5] improving mechanical system simulations [6], biological system analysis [7–10], and Micro and Nano Electromechanical Systems [11,12]. Despite the numerous efforts for reliably estimating damping parameters, the ability of engineers and scientists to use signal processing techniques to determine these parameters is ever improving as new and more sophisticated data analysis techniques are discovered.

* Corresponding author.
E-mail address: myersau3@msu.edu (A.D. Myers).

https://doi.org/10.1016/j.ymssp.2022.109042
Received 1 March 2021; Received in revised form 28 January 2022; Accepted 10 March 2022
Available online 4 April 2022

A common method for damping parameter identification is through a time domain analysis of the amplitude decrement (i.e. the damping envelope). This form of analysis is often implemented for viscous damping estimation through the logarithmic decrement of peaks. Unfortunately, many systems have nonlinear damping or large viscous damping thus preventing the use of the log decrement method. Additionally, when significant noise is present in the signal, the estimation of peak values requires a specific level of user expertise or subjective judgement, which makes damping parameter identification difficult to implement. These common issues have pushed researchers to develop automatic, noise robust methods for estimating damping parameters [13,14].

In the past decade, several methods have been developed for identifying systems parameters for a single degree of freedom system, including damping constants. These methods are typically based on either time domain or frequency domain analysis (i.e. modal analysis) of the oscillator. The time domain response methods for damping parameter estimation are typically based on analyzing the envelope of the free response decrement or through an energy balance approach. The envelope of the free response is commonly used for estimating damping parameters through an exponential envelope (viscous damping) or a constant decrement envelope (Coulomb or dry friction damping). Additionally, systems with both Coulomb and viscous damping can be simultaneously analyzed using vibration decrements in the time domain [15].

An analysis of the damping envelope can be applied to ambient vibration problems using the random decrement technique [16] where the input stochastic forcing function cannot be measured. The resulting random decrement signature encapsulates the damping information, which is typically extracted using the logarithmic decrement technique for viscous damping. One pitfall of this application is the possible spurious nonlinear behavior such as drift in the signature that can cause inaccurate estimates [17]. For multi-degree of freedom systems it is typical to use experimental modal analysis techniques such as the (Enhanced) Frequency Domain Decomposition [18,19], the Stochastic Subspace Decomposition [20–22], or Smooth Orthogonal Decomposition [23].

As an alternative to analyzing the envelope, the energy loss can be studied to estimate the damping parameters through least squares fitting for forced vibrations [24,25]. However, this approach requires forcing the oscillator to estimate the damping parameters, which is not always available or feasible. There are also energy-balance techniques for parameter identification that do not require forcing, but rather both the position and velocity signals [26]. However, this technique requires filtering the signal (e.g., using cubic spline fitting as in [26]), which adds pre-processing steps and can cause signal distortion. Another approach is to use the instantaneous energy dissipation [27], but this method requires a lightly damped system which is a significant, albeit common, limitation. There are also several other time domain methods including one based on areas [28], which requires viscous damping. This method numerically integrates the signal along segments between consecutive zero crossings allowing it to identify higher damping ratios than what is possible by the logarithmic decrement method. However, the approach in [28] replaces the problem of identifying noisy peaks with the arguably equivalent problem of identifying noisy zero crossings. Another commonly used method for parameter identification is to fit a function to the time series based on tuning the parameters of an analytical model; however, this requires an initial guess for all parameters and the convergence of an optimization algorithm. Another possible method for damping parameter estimation is based on solving a parabolic-type partial differential equation for the analysis of the inverse vibration problem to estimate both stiffness and damping [29]. However, this method requires both position and velocity data and is only resilient to moderate levels of noise.

As an alternative to time domain analysis, frequency response methods are typically applied by externally forcing the oscillator and measuring the phase and amplitude of the response at resonance (e.g. half-power method [30]). However, this assumes that the range of operation is within the linear region of oscillations or that the damping mechanisms are amplitude independent. This technique also requires a method of forcing the oscillator at multiple frequencies, which is not always feasible. An alternative to this option is to analyze the frequency response of a damped oscillation through the Fourier spectrum [31]. This method has been shown to be robust to some degree of additive Gaussian noise [32]. However, it requires a least-squares estimation algorithm applied to the frequency domain of the signal, which is an additional computational expense.

In some important practical applications, damping is the primary source of nonlinearities. For example, nonlinearities in structural damping predominantly appear in the damping term [33]. More specifically, jointed or built-up structures were shown to have power law dissipation, or equivalently that damping is a power law, and that their modes are preserved. Therefore, the modes' preservation in combination with power law dissipation necessitate the development of methods that can estimate damping in models where the sole source of nonlinearity is power law damping.

To fill this research gap, we describe a new approach that can be used for estimating damping in this class of models, and we specifically apply it to systems with viscous, Coulomb, or quadratic damping. To estimate the damping model that is most suitable out of those three damping mechanisms, our approach implements zero-dimensional (0D) sub-level set persistence, a tool from Topological Data analysis (TDA), to analyze the time domain response of a free vibration single degree of freedom oscillator. Our method extends the class of envelope analysis methods through a unique and noise robust analysis. Sublevel set persistence analysis also has the advantage of not requiring zero-centered signals or low damping, and is robust to non-stationarity in the signal. These are advantages over many common damping parameter estimation techniques that require at least a subset of these conditions [34]. We further show that our method is robust for a wide range of damping parameters (e.g., up to critical viscous damping), low sampling frequencies, and a high level of additive noise. Additionally, the algorithm for calculating the sublevel set persistence for one dimensional signals has a low computational cost, $O(nlog(n))$ as described in Algorithm 1, which is equivalent to the fast Fourier spectrum [35].

Sublevel set persistence has recently been shown as a robust data analysis tool through applications ranging from step detection [35] to cancer histology [36]. One of the most attractive features of sublevel set persistence is its robustness to perturbations (see stability theorem [37]). Additionally, by using sublevel set persistence to analyze the time domain of the free

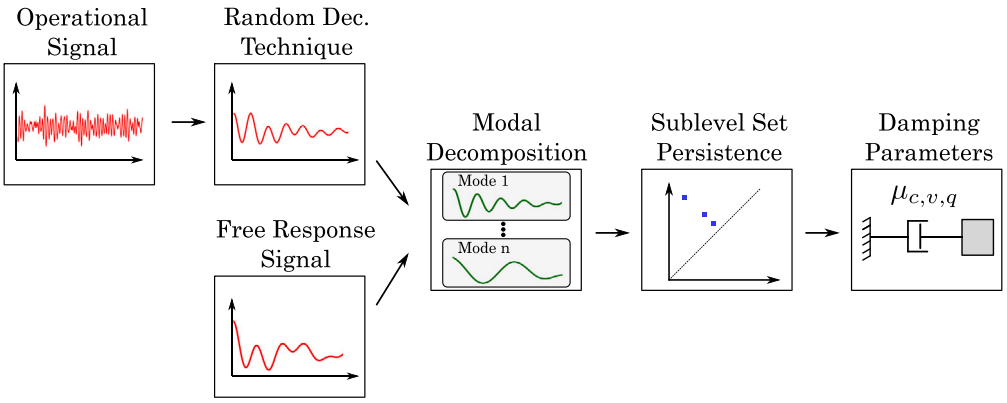

Fig. 1. Pipelines for our applying our sublevel set persistence approach for damping parameter estimation to either an operational signal via the random decrement technique or the free response signal. The resulting damping signature is analyzed using modal decomposition which allows for the use of our sublevel set persistence approach to estimate the damping parameters.

responses of a damped oscillator we will later be able to analyze the full domain (including non-linear responses) of the system similar to the work done in analyzing MEMS [11].

Our method is designed for the analysis of the amplitude decrement profile or signature for estimating the damping parameters of the system. The most direct method for getting this signature is through the free response signal. However, it is often necessary to estimate the damping parameters through the use of only an operational signal where the underlying system responds to ambient excitation such as Gaussian noise. A common solution for the analysis of these signals is to use the random decrement technique [16]. The random decrement technique extracts a damping signature from the signal that represents a decay function, which can then be analyzed using our sublevel set persistence approach to estimate the damping parameters. Therefore, our approach can also be used within the framework of operational modal analysis.

Although we present our method using example one-degree-of-freedom system, our approach is extensible to multiple degree of freedom systems. Specifically, by leveraging modal decomposition techniques for breaking down the signal into its modal components, each mode's decrement signature can be studied using our approach. The signal can be decomposed using tools such as the frequency domain decomposition [18,19], stochastic subspace decomposition [20–22], smooth orthogonal decomposition [23], short-time Fourier transform, empirical mode decomposition, Hilbert transform, and wavelets [38]. Alternatively, in [39] an approach using Band-Pass Filtering (BPF) around each natural frequency is used to separate each of the modal responses in lightly damped, multi-degree of freedom systems with weak nonlinearity and well-separated natural frequencies. Our approach can then be used on the separated modes to extract the corresponding modal damping as illustrated in the free response signal pipeline in Fig. 1. If we are working with an operational signal from a multi-degree of freedom system (commonly known as an operational modal analysis problem) we can apply the random decrement technique first to generate a random decrement signature. The signature can then be analyzed using a modal decomposition technique such as a Fourier transform analysis used in [40]. Our sublevel set persistence technique can then be applied to operational modal analysis problems using the sublevel set persistence of each mode's signal as shown in the operational signal route of the pipeline in Fig. 1.

1.1. Organization

This paper is ordered as follows. First, in Section 2 an introduction to TDA and sublevel set persistence is provided. Following this, in Section 3 the closed form solutions (if applicable) and background information for viscous, Coulomb and quadratic damping are summarized. Section 3 also leverages the solutions to the damped responses for use with sublevel set persistence for damping identification. In Section 4 we begin an analysis of the effects of noise on damping parameter identification using sublevel set persistence. This analysis introduces two methods for minimizing the effects of noise. The first is based on a statistical analysis of additive noise in the persistence domain and the second is based on a function fitting approach. In Section 5 we provide three examples demonstrating each damping mechanism. Finally, the results section (Section 6) showcases our method using a wide range of damping parameters, noise levels, and sampling frequencies. To make replicating this work easier for readers, the Python code for automatically calculating the damping parameters and constants has been made publicly available through GitHub (*github.com/Khasawneh-Lab*).

1.2. Problem statement and our contribution

A single degree of freedom system subject to a general damping term can be written as

$$m\ddot{x}(t) + h(\dot{x}) + kx(t) = 0, \tag{1}$$

where m is mass, c_n is the damping coefficient, and k is stiffness. We consider damping terms proportional to the nth power of velocity $h(\dot{x}) = c_n|\dot{x}^{n-1}(t)|\dot{x}(t)$ with $n \in \{1,2\}$ corresponding to viscous and quadratic damping, respectively, as well as damping given by a piecewise linear function $h(\dot{x}) = c\,\text{sign}(\dot{x})$ representing Coulomb damping.

Model (1) where the prominent source of nonlinearity is due to the nonlinear damping term is of interest in practical systems [41]. The energy dissipation described by the function $h(\dot{x})$ is practically captured experimentally, for example by recording the free response of the system. In this setting, we have a time series $s(t)$ that contains *observations* of the actual response $x(t)$ but with additive, typically Gaussian, measurement noise. For a limited number of choices for the damping function $h(\dot{x})$, there exists methods for extracting the damping parameter from the response data with the most notable ones corresponding to viscous, Coulomb, and quadratic damping. However, these methods require a filtered signal, so the user must first remove noise thus adding extra processing time and introducing the possibility of signal distortion. In addition some of these methods can only be used to estimate the damping parameter on a subset of its domain. For example, the logarithmic decrement approach, which is widely used to estimate viscous damping coefficients, is limited to damping ratio values below 0.3 although an oscillatory system can have damping ratios that go up to one. Therefore, there are two challenges for estimating damping from oscillatory signals: extracting a noise-free representation of the signal without altering the signal characteristics or requiring high level of user expertise, and estimating the damping parameters from the resulting representation for common damping models over the full range of interest.

We introduce for the first time an approach based on Topological Signal Processing (TSP) for estimating the damping coefficient from time series with additive noise whose underlying dynamics are described by (1) for $n \in \{1,2\}$, or with Coulomb damping $h(\dot{x}) = c\,\text{sign}(\dot{x})$. A distinguishing feature of our approach is that it only requires the raw, free decay signal with additive iid noise as input, although we restrict our presentation to the practical case of additive white noise. We also deduce using the stability theorem of persistence diagrams [37] that the persistence diagram representation for Eq. (1) with power-law nonlinearity in the damping term is also stable in the sense that small perturbations of $x(t)$ lead to small perturbations in the sublevel set persistence relative to the noise-free case. The authors' prior work [42] showed that generally if noise corresponds to iid samples then the persistence diagram separates the noise from the signal using a threshold that depends on the noise distribution (the authors provided threshold values for common noise models such as Gaussian, uniform, exponential and Rayleigh distributions). Therefore, our approach provides a filter-free tool with minimal user input for estimating damping in single degree of freedom systems from their raw signals contaminated by additive noise with bounded or strongly concentrated distribution even when the damping term is nonlinear (quadratic damping) or the resulting equation of motion is piecewise linear (Coulomb damping). We also describe a framework for selecting the most probable damping model in Section 3.4 when the most likely damping mechanism is not known a-priori, but it fits one of the three common damping mechanisms (Coulomb, viscous, or quadratic).

2. Topological data analysis

In this work we use topological Data Analysis (TDA) [43] as our main tool for analyzing the amplitude decrement of the damped free-oscillations from the spring mass damper shown in Fig. 4. TDA is a method of data analysis from mathematics used to study datasets from the perspective of topology or shape. Although TDA can be used to study different types of data inputs including data in high dimensional Euclidean spaces, we only need to utilize it to study 1D time series so we will restrict our presentation to that case. Studying the shape of data through the persistent homology of embedding point clouds from a time series has been successfully used for periodicity quantification through signal analysis [44], detecting quasi-periodicity in video data [45], chatter detection in turning processes [46,47], stability of delayed equations [48], and complex network analysis [49].

Sublevel set persistence can also be used as a time series analysis tool by measuring the significance of the sublevel sets as we show in the following section. Sublevel set persistence has been successfully implemented for a wide range of time series analysis applications including local extrema detection [50], true step detection in signal processing [35], Fourier spectrum analysis [51], and cancer histology [36]. In this work we are interested in analyzing the amplitude decrement of a time series; therefor, sub-level set persistence will be the tool that we will use in this work.

2.1. Sublevel set persistence

This section provides a basic introduction to sublevel set persistence, but a more thorough background on TDA and its several commonly used tools can be found in [52–54]. Let us begin with the real-valued single variable function $f : \mathbb{R} \to \mathbb{R}$ with critical points at the local extrema. For our setting, we define the sublevel set for f at level $\alpha \in \mathbb{R}$ as the set $\mathbf{S}_\alpha = \{x|f(x) \leq \alpha\}$, and we show how the corresponding sublevel persistence is computed using the example shown in Fig. 2.

Given a function such as the one shown in Fig. 2A and Fig. 3, we start calculating the sublevel set persistence by setting $\alpha = -\infty$. For our application we extend the right end of the signal to $-\infty$ and assume that the first element in our sublevel set is born there. We then visualize water level rising on top of the curve of f along the y axis with the value of α increasing as shown by the shading in Fig. 2. We then increment α so that its value lands at the next local extrema since these are the points where significant changes occur in the sublevel set. At the first extrema labeled v_0 in Fig. 2A, we see that a new, disjoint pool of water starts to emerge. When a new pool of water appears, we say that a 0D class was born in the persistence diagram, in this case at level v_0. By increasing the filtration to $\alpha = v_1$ in Fig. 2B, another pool starts to fill in at v_1, thus leading to the birth of third persistence class at v_1. Note that at level $\alpha = v_1$, the first and second pools are persisting so we have a total of three 0D classes that were born. In contrast, in Fig. 2C when we reach the local maximum $\alpha = p_0$ two of the pools connect. When this happens, the class that was born earlier (i.e., the pool that showed up first) persists while the set that was born later dies according to the Elder's Rule [55]. So in Fig. 2C the 0D class

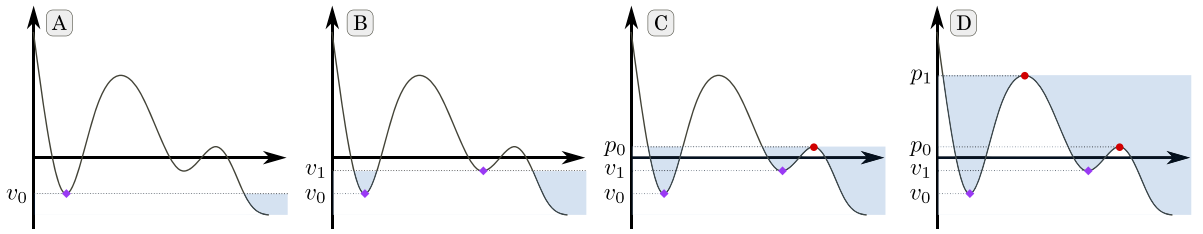

Fig. 2. Example 0D sub-level set persistence from function $x(t)$ (top left) with the resulting persistence diagram (top right) and time ordered lifetimes (bottom).

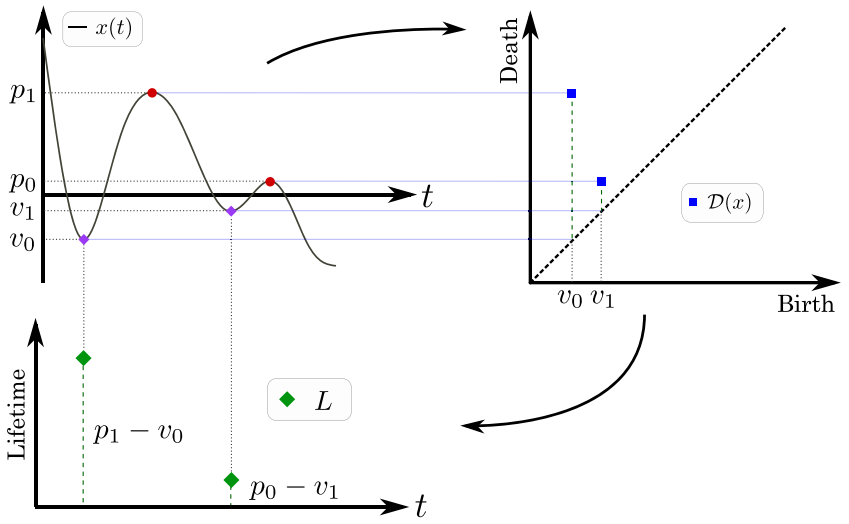

Fig. 3. Example 0D sub-level set persistence from function $x(t)$ (top left) with the resulting persistence diagram (top right) and time ordered lifetimes (bottom).

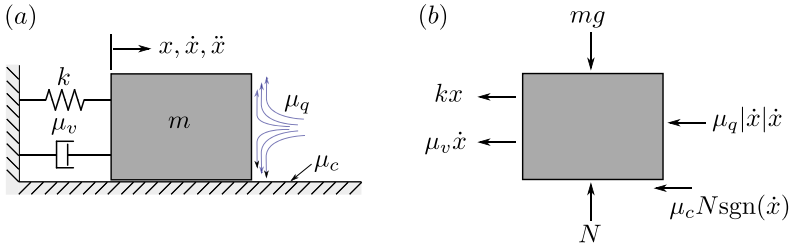

Fig. 4. Single degree of freedom oscillator with multiple modes of energy dissipation. Energy dissipation mechanisms include Coulomb μ_c, viscous μ_v, and quadratic μ_q damping.

that was born at $-\infty$ persists, while the one that was born at v_1 dies. The collection of (birth,death) pairs for each class constitutes the coordinates for points in what is called a persistence diagram, which is a 2D representation that tracks the birth and deaths of features as a function of α. So for this example, a point with coordinates (v_1, p_0) is added to the persistence diagram as shown in Fig. 3. From here no fundamental changes in the structure of the pools occurs until reaching $\alpha = p_1$, where the other sublevel set born at v_1 dies visualized as the overflowing of the second pool in Fig. 2D.

The birth and deaths of the two persistence pairs are recorded in the persistence diagram on the right side of Fig. 3 as the points (v_0, p_1) and (v_1, p_0). As shown in the persistence diagram the point (v_1, p_0) is close to the diagonal which signifies that the sub-level set only persisted for a short range in α, while the point (v_0, p_1) is far from the diagonal suggesting it was from a significant sub-level set. We can summarize the significance of points in a persistence diagram using their lifetimes $L = \alpha_D - \alpha_B$. The third persistence pair never dies as it was from an infinite class and would be plotted at $(-\infty, \infty)$ in the persistence diagram. However, since infinite class persistence pairs are not of consequence in this work we will ignore them in the subsequent work. To use sublevel set persistence in practice we have provided the $O(n \log n)$ algorithm for calculating the sublevel set persistence in the Appendix, which was originally developed in [42].

In this work, we will also use a new representation of a persistence diagram from sublevel sets of a time series, This method is specifically useful for time series analysis. We call this representation the time ordered lifetimes plot, which is formed by first

calculating the lifetimes from the persistence diagram as $L = \alpha_D - \alpha_B$. In addition to the lifetimes, we need to track the time t_{B_i} when each lifetime L_i is born (occurs at local minima v_i) as shown in the bottom of Fig. 3.

The stability of persistence diagrams to small perturbations in the input data was shown for a general setting in [37]. Here we are interested in the specific setting of a time series $x(t) : \mathbf{R} \to \mathbf{R}$ that describes the response of the underlying model (1), subject to small perturbations due to additive (white) noise. We show the stability of persistence in this setting as a corollary to the main theorem in [37]. The key observation is that for systems described by model (1) where nonlinearity is only in the damping term the resulting response exhibits no jumps or bifurcations [41]. The same is true for Coulomb damping where the dissipation term is described by a piecewise linear function and the response is continuous.

Define the bottleneck distance $d_B(X, Y) = \inf_\gamma \sup_x \|x - \gamma(x)\|_\infty$, where $x \in X$ and $y \in Y$ range over all points and γ ranges over all bijections from X to Y allowing matching to the diagonal. The stability theorem in [37] restricted to our setting then applies and it reads

Theorem 1. *Given continuous functions with finitely many critical points $f, g : \mathbb{R} \to \mathbb{R}$, then the persistence diagrams $D(f)$ and $D(g)$ satisfy $d_B(D(f), D(g)) \leq \|f - g\|_\infty$.*

We further add that if the perturbations correspond to bounded or strongly concentrated distributions such as Gaussian noise, then the homology is not strongly affected by the perturbations [56,57].

3. Sublevel set persistence of damping mechanisms

In this section we introduce three damping mechanisms commonly used: Coulomb, viscous, and quadratic. For each form of damping, a theoretical relationship between the theoretical consecutive persistence pairs is formulated and used to determine the underlying damping parameter of the system.

The results in this paper will be generated from both experimental data and numerically simulated single-degree-of-freedom spring–mass system with three common forms of power-law damping (see Fig. 4): Coulomb, viscous, and quadratic. The forces caused by each of the damping mechanisms are applied to Newton's law to generate an equation of motion as

$$m\ddot{x} = -kx - \mu_c N|\dot{x}|\text{sgn}(\dot{x}) - \mu_v\dot{x} - \mu_q|\dot{x}|\dot{x}, \tag{2}$$

with a mass m, spring constant k, and normal force $N = mg$. Here the normal force is constant, but in many applications this will not be the case, which can leave $N = f(\ddot{x}, \dot{x}, x)$ where x is the position of the system and $\dot{}$ are its time derivatives.

3.1. Viscous damping

If the system being analyzed is assumed to be dominated by viscous damping then the system model is reduced from Eq. (2) to $m\ddot{x} + kx + \mu_v\dot{x} = 0$. This linear differential equation has the closed form solution as

$$x(t) = Ae^{-\zeta_v\omega_n t}\cos(\omega_d t - \phi), \tag{3}$$

where the viscous damping can be summarized using the damping ratio $\zeta_v = \mu_v/(2\sqrt{mk})$, the natural frequency $\omega_n = \sqrt{k/m}$, the damped natural frequency $\omega_d = \omega_n\sqrt{1-\zeta_v^2}$, the phase shift ϕ, and the initial amplitude of the time series A. Typically, ζ_v is estimated using local maxima and the log decrement method as

$$\zeta_v = \sqrt{\frac{1}{1 + \left(\frac{2\pi n}{\ln\left(\frac{p_i}{p_{i+n}}\right)}\right)^2}}, \tag{4}$$

where p_{i+n} and p_i denote the $(i+n)$th and ith peaks, respectively. Unfortunately, this method for estimating ζ_v is difficult to implement in an automatic way when noise is present as the selection of peaks becomes difficult. Additionally, if the time series is non-stationary or does not have a zero-mean, the standard logarithmic decrement method will not provide accurate damping parameter estimates. To help combat these issues we will implement sub-level set persistence to show how ζ_v can be calculated from the resulting persistence diagram.

Let us begin with a toy example of the time series and the resulting persistence diagram for viscous damping as shown in Fig. 5. The x and y coordinates in the persistence diagram correspond to the local minima v_n and maxima p_{n+1} in the time series $x(t)$. From the known, closed-form solution in Eq. (3), the values of the peaks and valleys are solved for as

$$p_i = Ae^{-\zeta_v(2i\pi+\phi)/\sqrt{1-\zeta_v^2}} \tag{5}$$

and

$$v_i = -Ae^{-\zeta_v(2i\pi+\pi+\phi)/\sqrt{1-\zeta_v^2}}, \tag{6}$$

respectively. From the peaks and valleys or births and deaths for the persistence pairs, their lifetimes are calculated as

$$L_i = p_{i+1} - v_i = Ae^{\frac{-i\zeta_v 2\pi}{\sqrt{1-\zeta_v^2}}}\left(e^{\frac{-\zeta_v 2\pi}{\sqrt{1-\zeta_v^2}}} + e^{\frac{-\zeta_v\pi}{\sqrt{1-\zeta_v^2}}}\right), \tag{7}$$

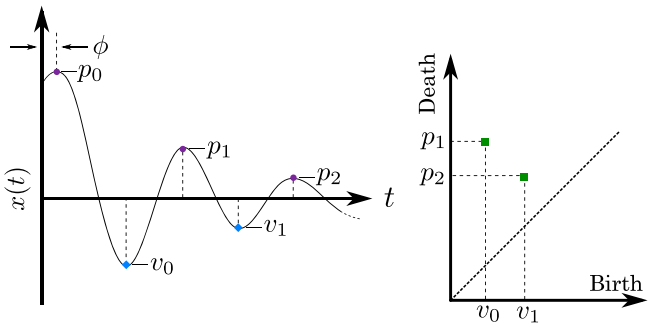

Fig. 5. Example 0D sub-level set persistence from the viscous damped free response time series $x(t)$.

where L_i is a lifetime of the sub-level set persistence pair (v_i, p_{i+1}). repeating this lifetime calculation for the $(i+n)$th peak–valley pair results in another lifetime L_{i+n}, which is used to find the ratio between lifetimes as

$$\frac{L_{i+n}}{L_i} = e^{-n\zeta_v 2\pi/\sqrt{1-\zeta_v^2}}. \tag{8}$$

By taking this ratio, the amplitude A cancels out, which allows for Eq. (8) to be used to calculate ζ_v as

$$\zeta_v = \sqrt{\frac{1}{1+\left(\frac{2n\pi}{\ln(L_{i+n}/L_i)}\right)^2}}, \tag{9}$$

From the damping ratio we can also calculate the viscous damping constant as $\mu_v = 2\zeta_v\sqrt{km}$ if the other system parameters m and k are known. Another benefit of using sublevel set persistence for estimating the damping ratio is that only a single lifetime is needed. The standard method for estimating ζ_v in Eq. (4) needs atleast two peaks to estimate the damping ratio, while only a single lifetime is needed for estimating the damping constant with a slight variation of Eq. (9). Specifically, if we assume the time series $x(t)$ is centered about zero such that $\lim_{t\to\infty} x(t) = 0$, then we use the v_0 and p_1 to calculate the damping ratio as

$$\zeta_v = \sqrt{\frac{1}{1+\left(\frac{\pi}{\ln(-p_1/v_0)}\right)^2}}, \tag{10}$$

It should be noted that this method does require a first valley, which results in a damping ratio $\zeta_v < 1$. If $\zeta_v > 1$, then the damping is considered over-damped and the method will not work to estimate the damping ratio.

Using the sublevel set persistence we can also calculate the damped frequency using ordered time indices at which each of the sublevel sets was born as $t_B = [t_{v_0}, \ldots, t_{v_n}]$. The frequency is then calculated as the reciprocal of the median difference in time between t_{v_i} and $t_{v_{i+1}}$.

3.2. Coulomb damping

To determine a method for relating the lifetimes to the Coulomb damping constant μ_c and Coulomb damping parameter ζ_c, we must first determine a theoretical expression for the response of a spring mass damper with only Coulomb damping. To do this, we will implement the method defined in [58]. However, we do acknowledge other methods for analyzing Coulomb damping (i.e. an energy approach [59]). Let us begin by defining the equation of motion from Eq (2) with $\mu_v = \mu_q = 0$, resulting in $m\ddot{x} = -kx - \mu_c N\text{sgn}(\dot{x})$. The solution to this differential equation is solved by breaking the system into two different states: (1) $\dot{x} > 0$ or (2) $\dot{x} < 0$, which each result in a unique (linear) differential equation. By "stitching" these solutions together we can get the solution as

$$x(t) = (A - \frac{2\mu_c N\omega_n}{\pi k}t)\cos(\omega_n t - \phi), \tag{11}$$

which has a linear amplitude decrement while $|A(1 - \frac{2\mu_c N\omega_n}{\pi k}t)| > \mu_s N/k$ with the phase shift ϕ introduced from other initial conditions. If the inequality is broken at sticking time t_s, then

$$x(t > t_s) = (A - \frac{2\mu_c N\omega_n}{\pi k}t_s)\cos(\omega_n t_s - \phi) \tag{12}$$

An example of this linear decrement and the sticking condition are shown in Fig. 6.

We now leverage this closed form solution to be used with sublevel set persistence. To do this we start by shifting Eq. (11) to have $t = \tau$, where τ is the time at the first valley or $\tau = (\phi - 1)/\omega_n$, which results in the shift form of the equation of motion as

$$x(\tau) = (A - \frac{2\mu_c N\omega_n}{\pi k}\tau)\cos(\omega_n \tau). \tag{13}$$

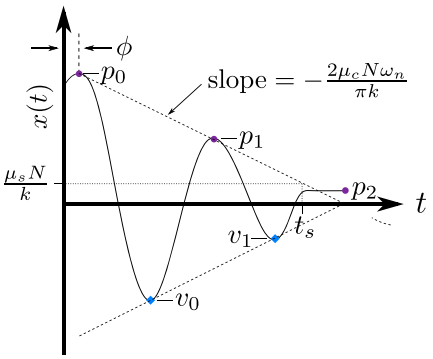

Fig. 6. Example free vibration response of system with Coulomb damping.

From Eq. (13), the peaks p_i occur at $\tau = 2i\pi/\omega_n$ and have values of $p_i = A - 4i\mu_c N/k$, and the valleys v_i occur at $\tau = \pi(2i+1)/\omega_n$ with values of $v_i = 2(2i+1)\mu_c N/k - A$. The lifetime of the resulting persistence pairs are calculated as

$$L_i = p_{i+1} - v_i = 2A - \frac{(8i+6)\mu_c N}{k}. \tag{14}$$

Extending Eq. (14) to a second persistence pair results in the lifetime L_{i+n}, which is used to cancel the amplitudes with $L_{i+n} - L_i = \frac{-8n\mu_c N}{k}$. This difference is then used to solve for the Coulomb damping constant as

$$\mu_c = \frac{k(L_i - L_{i+n})}{8nN}. \tag{15}$$

With an expression for μ_c, the Coulomb damping parameter ζ_c is estimated since it is independent of other system parameters (N and k). This parameter is the magnitude of the slope of the decrement and is solved for using Eq. (15) as

$$\zeta_c = \frac{2\mu_c N\omega_n}{\pi k} = \frac{\omega_n(L_i - L_{i+n})}{4n\pi} = \frac{(L_i - L_{i+n})}{2(t_{B_{i+n}} - t_{B_i})}, \tag{16}$$

where t_{B_i} is the time when L_i was born or at the time index of the local minima. Similar to Viscous damping, we can also use a single lifetime to estimate both μ_c and ζ_c. To do this, we again assume that the time series $x(t)$ is zero centered. If so, the damping constant and parameter are calculated as

$$\mu_c = -\frac{k(v_0 + p_1)}{2N} \tag{17}$$

and

$$\zeta_c = \frac{2\mu_c N\omega_n}{\pi k} = -\frac{\omega_n(v_0 + p_1)}{\pi} = \frac{v_0 + p_1}{t_{v_0} - t_{p_1}}, \tag{18}$$

where t_{p_1} and t_{v_0} are the time indices at the local maxima and minima, respectively.

If the damping mechanism of a system is dominated by both viscous and Coulomb damping we suggest implementing the amplitude decrement described by Liang and Feeny [15] in combination with sublevel set persistence.

3.3. Quadratic damping

For quadratic damping, Eq. (2) is reduced to $m\ddot{x} = -kx - \mu_q \text{sgn}(\dot{x})\dot{x}^2$, which is a non-linear differential equation that does not have a closed form solution. However, there is a solution for calculating the turning points of the solution $x(t)$ [60]. For estimating the damping constant μ_q and the associated parameter ζ_q we use these turning points, which are determined by first splitting the equation of motion into two states as

$$0 = \begin{cases} \ddot{x} + \frac{\mu_q}{m}(\dot{x})\dot{x}^2 + \frac{k}{m}x, & \dot{x} > 0 \\ \ddot{x} - \frac{\mu_q}{m}(\dot{x})\dot{x}^2 + \frac{k}{m}x, & \dot{x} < 0. \end{cases} \tag{19}$$

Similar to the solution method for Coulomb damping, quadratic damping requires the solution to be solved Iteratively between the two possible equations of motion in Eq. (19) as $\text{sgn}(\dot{x})$ alternates. Fay [60] uses an integration multiplier to show that the differential equation

$$\ddot{x} + p(x)\dot{x}^2 + f(x) = 0 \tag{20}$$

has the solution form

$$\mu(x)\frac{y^2}{2} + \int_{x_0}^{x} \mu(\epsilon)f(\epsilon)d\epsilon = \frac{y_0^2}{2}\mu(x_0), \tag{21}$$

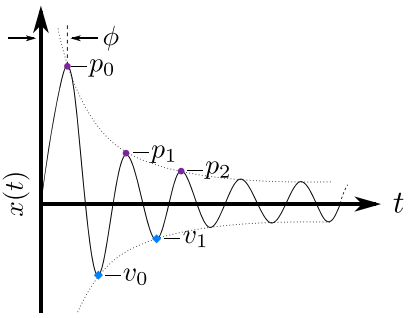

Fig. 7. Example free vibration response of system with quadratic damping.

where $\mu(x) = e^{\int 2p(x)dx}$. By applying this solution to the equation of motion with $p(x) = \pm\mu_q$ (the $\pm$ represents the two possible conditions with + if $\dot{x} > 0$), $\mu(x) = e^{\pm 2\mu_q x/m}$, and $f(x) = kx$, we solve the equation as

$$\frac{\dot{x}^2}{2} e^{\frac{\pm 2\mu_q}{m} x} + \frac{k}{m} \int_{x_0}^{x} e^{\frac{\pm 2\mu_q}{m} \epsilon} \epsilon d\epsilon = \frac{\dot{x}_0^2}{2} e^{\frac{\pm 2\mu_q}{m} x_0}. \tag{22}$$

The integral is then solved using the method of integration by parts as

$$\left(\dot{x}^2 + \frac{k\left(x - \frac{m}{\pm 2\mu_q}\right)}{\pm\mu_q} \right) e^{\frac{\pm 2\mu_q}{m} x} = \left(\dot{x}_0^2 + \frac{kx_0}{\pm\mu_q} - \frac{km}{2\mu_q^2} \right) e^{\frac{\pm 2\mu_q}{m} x_0}. \tag{23}$$

Eq. (23) is then numerically solved using iteration as the solution goes through $\dot{x} = 0$. However, we would like to use an expression for the relationship between a valley and the following peak to understand how the lifetimes decrease due to the quadratic damping mechanism. To do this we first assume any initial condition $[|x_0|, |\dot{x}_0|] \neq \mathbf{0}$, which will yield a solution $x(t)$ that will eventually go to a valley. We then consider the new initial condition $\mathbf{x}_0' = [v_0, +0]$ at this first valley v_0 (see Fig. 7 for a sample response with non-zero initial conditions). The velocity is positive ($\dot{x} > 0$) between this first valley v_0 and until the next peak p_1. Therefor, we can use Eq. (23) with $+\mu_q$ to solve for the relationship between any valley and peak pair as

$$e^{\frac{2\mu_q}{m} p_{i+1}} \left(p_{i+1} - \frac{m}{2\mu_q} \right) = e^{\frac{2\mu_q}{m} v_i} \left(v_i - \frac{m}{2\mu_q} \right). \tag{24}$$

This relationship can be rearranged as

$$L_i = p_{i+1} - vi = \frac{m}{2\mu_q} \ln\left(\frac{2\mu_q v_i - m}{2\mu_q p_{i+1} - m} \right). \tag{25}$$

After applying sublevel set persistence and generating a persistent diagram, values for the lifetimes, valleys, and peaks are known, which allows for the numerical estimation of μ_q. This is done by minimizing the cost function

$$C(\mu_q) = \left[L_i - \frac{m}{2\mu_q} \ln\left(\frac{2\mu_q v_i - m}{2\mu_q p_{i+1} - m} \right) \right]^2. \tag{26}$$

where $C(\mu_q)$ is the cost as a function of μ_q. We can now also introduce the quadratic damping parameter $\zeta_q = \mu_q/m$. Applying ζ_q to Eqs. (26) results in

$$C(\zeta_q) = \left[L_i - \frac{1}{2\zeta_q} \ln\left(\frac{2\zeta_q v_i - 1}{2\zeta_q p_{i+1} - 1} \right) \right]^2. \tag{27}$$

which now has no needed system parameters m and k. Eq. (27) can also be numerically minimized to estimate ζ_q.

3.4. Identification of Coulomb, viscous or quadratic damping

An underlying requirement in many methods for estimating the damping parameter is that the type of damping mechanism is known or can be guessed based on experience. However, it is often the case that the damping mechanism cannot be identified through either a visual inspection of the signal or through a prior knowledge on the source of energy loss. To alleviate this issue we provide an empirical method for automatically selecting the damping mechanism based on a comparison between simulated and collected signals. This process is based on using the estimated damped frequency ω_d and the damping ratio for Coulomb, viscous, and quadratic damping (ζ_c, ζ_v, and ζ_q) from the signal. Using these estimated parameters we can simulate a signal using an initial condition. A typical choice for initial conditions for experimental data is at the first peak where the conditions are approximately $[x(0), \dot{x}(0)] = [X_0, 0]$. We can then compare the simulated and real signal using the Root Mean Square Error (RMSE) to make a conclusion on which damping mechanism provided the closest match. This process is outlined as follows:

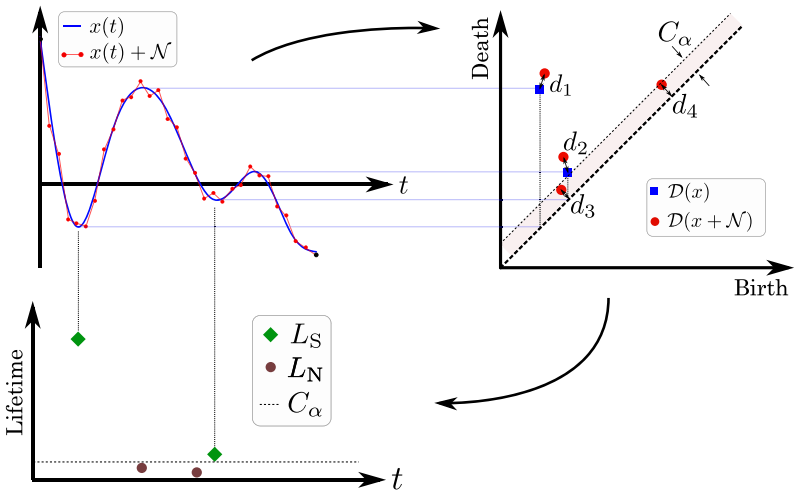

Fig. 8. Sub-level set persistence applied to sample time series $x(t)$ with and without additive noise $\mathcal{N}$. This demonstrates the robustness of persistent homology with the time series (top left) with and without additive noise and the small effect on the resulting persistence diagrams (top right) and the corresponding time ordered lifetimes (bottom left).

1. Estimate ω_d and ζ_c, ζ_v, ζ_q from the signal using sublevel set persistence.
2. Calculate ω_n using ω_d for each of the three damping mechanisms and set the initial conditions from the first peak as $[x(0), \dot{x}(0)] = [X_0, 0]$.
3. Modify recorded signal to start at the first peak.
4. Simulate or use the solved equation of motion for each damping type:
   - Coulomb: $x(t) = (X_0 - \zeta_c t)\cos(\omega_n t)$
   - Viscous: $x(t) = X_0 e^{-\zeta_v \omega_n t}\cos(\omega_d t)$
   - Quadratic: $\ddot{x} + \zeta_q \text{sgn}(\dot{x})\dot{x}^2 + \omega_n^2 x = 0$
5. Calculate the RMSE between each simulated signal and the collected signal.
6. Choose the damping model with the smallest RMSE.

An example implementing this damping mechanism selection process is demonstrated for experimental data in Section 5.2. We note here that we estimate the natural frequency ω_n for quadratic damping as the damped frequency ω_d due to the results found in [61] showing that the frequency of the quadratically damped oscillator approaches the natural frequency.

4. Noise compensation

While we have already developed expressions for estimating the damping parameters and constants from sublevel set persistence in Section 3, we need to develop an automatic framework for the method to be applied to real-world signals with inherent noise. To illustrate the effects of noise, let us return to our example sublevel set persistence from Fig. 3, but with additive noise, so our observed signal is $x(t) + \mathcal{N}$. The resulting persistence diagrams from sublevel set persistence from the time series without $\mathcal{D}(x)$ and with additive noise $\mathcal{D}(x + \mathcal{N})$ are shown in Fig. 8 as well as the resulting time ordered lifetimes. This example shows that the addition of noise does not have a large effect on the position of significant sublevel sets in the persistence diagram with the distances between significant points (d_1, d_2, d_3, d_4) all being relatively small. This is no surprise due to the stability theorem of persistence diagrams [37].

While we know that the resulting persistence diagrams will be stable, the additive noise does introduce several points in the persistence diagram located near the diagonal with relatively small lifetimes. These noise-artifact persistence pairs are formed from the peak–valley pairs in the additive noise. For our method of damping parameter estimation to function correctly, we needed to develop a method for dealing with these noise-artifact persistence pairs. One way of removing the noise-artifact persistence pairs is to separate significant and insignificant lifetimes through a confidence interval or cutoff. While there are methods for developing cutoffs based on a confidence set for persistence diagrams [62,63], these methods often require that the time series sampling frequency is significantly higher than the highest dominate frequency of the time series or that the persistence diagram is generated from persistent homology and not sublevel set persistence. Both of these issues make implementing these methods difficult for persistence diagrams generated from sublevel set persistence. Additionally, methods such as persistent entropy [64] for separating noise from significant features in a persistence diagram may not properly distinguish between the noise and significant points if the number of significant data points in the persistence diagram is relatively large compared to the amount of noise. To combat both of these issues, we will introduce two methods for estimating the damping constant with additive noise using sublevel set persistence.

Table 1
Cutoff and parameter estimation equations for the Gaussian, uniform, Rayleigh, and exponential probability distribution functions.

Distribution	Cutoff Equation C_α	Parameter Estimation
Gaussian	$1.923\tilde{L}\,\mathrm{erf}^{-1}\left[2(1-\sqrt{\alpha})^{1/n}-1\right]$	$\sigma \approx 0.680\tilde{L}$
Uniform	$2\tilde{L}\left[2\left(1-\sqrt{\alpha}\right)^{1/n}-1\right]$	$\Delta \approx 2\tilde{L}$
Rayleigh	$1.025\tilde{L}\left(\sqrt{-2\ln\left([1-\sqrt{\alpha}]^{1/n}\right)}-\sqrt{-2\ln\left(1-[1-\sqrt{\alpha}]^{1/n}\right)}\right)$	$\rho \approx 1.025\tilde{L}$
Exponential	$-0.533\tilde{L}\ln\left([1-\sqrt{\alpha}]^{1/n}-[1-\sqrt{\alpha}]^{2/n}\right)$	$\lambda \approx \frac{1.875}{\tilde{L}}$

Table 2
Constants of (28) for each distribution type investigated in this work with associated uncertainty from ten trials.

Distribution	Gaussian	Uniform	Rayleigh	Exponential
c_1	0.845 ± 0.029	0.880 ± 0.017	0.726 ± 0.026	0.436 ± 0.036
c_2	0.809 ± 0.061	0.639 ± 0.026	0.605 ± 0.054	0.393 ± 0.075

The first method is based on generating a confidence level based cutoff for the persistence diagram for sublevel set persistence, which is founded on the assumed theoretical probability distribution $f(x)$ of noise in the persistence diagram developed in [42]. This assumed distribution allows for an accurate cutoff separating noise from features based on a desired confidence level α.

The second method uses a dual function fitting algorithm applied to the time ordered lifetimes diagram. Specifically one curve is fit to the damping envelope of the lifetimes while the second is fit to the additive noise lifetimes. However, this method is only viable for viscous and Coulomb damping as the envelope function is unknown for quadratic damping.

The aforementioned methods will be developed and discussed in the proceeding sub-sections as follows. First, in Section 4.1 we will provide an overview of the recently developed and novel analysis of the statistics of the lifetimes in the persistence diagram [42] and how its resulting cutoff can be used to separate significant persistence pairs from those associated to noise in the persistence diagram. These significant persistence pairs can then be used to estimate the damping parameters as discussed in Section 3. In Section 4.2, we will introduce the method based on a dual curve fitting procedure in the time ordered lifetimes diagram to estimate the damping parameters.

4.1. Method 1: Persistence diagram cutoff

The first method is based on calculating a suitable cutoff to separate persistence pairs associated to additive noise from those of signal. To do this, we implement the recently published work on estimating a suitable cutoff for the persistence diagram (and time ordered lifetimes diagram) by assuming an additive noise distribution [42]. We overview the key results from this work in Section 4.1.1. We additionally develop a noise floor compensation term to minimize the effects additive noise has on the accuracy of the estimated damping parameters in Section 4.1.2. Finally, in Section 4.1.3 we show how the cutoff and noise floor are used to estimate the damping parameters.

4.1.1. Cutoff equations

For the method developed in [42], the cutoff equations require an assumed probability distribution function for the additive noise. Due to this constraint, we have provided four, commonly assumed probability distributions as Gaussian, uniform, Rayleigh, and Exponential distributions with their associated cutoff equations and approximated distribution parameters as shown in Table 1. From Table 1, $\tilde{L}$ is the median lifetime, n is the number of samples in the signal, α is the confidence level (this is usually chosen as 0.001), and σ, Δ, ρ, and λ are the distribution parameters for the Gaussian, uniform, Rayleigh, and exponential distributions, respectively. For the sake of brevity we will use the Gaussian example with distribution parameter σ.

To compensate for the effects of signal on the cutoff and parameter estimation equations, we suggest the use of the multiplication compensation term for the signal as R. This term is used to compensate for the effects of signal with $C_\alpha^* = RC_\alpha$ and $\sigma^* = R\sigma$ and is calculated as

$$R = e^{c_1\left(\frac{\delta}{\delta+\tilde{L}}\right)^{c_2}}, \tag{28}$$

where the two constants c_1 and c_2 are provided in Table 2 and δ is approximated as

$$\delta \approx \frac{2}{n}\sum L_{C_\alpha}, \tag{29}$$

with L_{C_α} as the lifetimes greater than C_α.

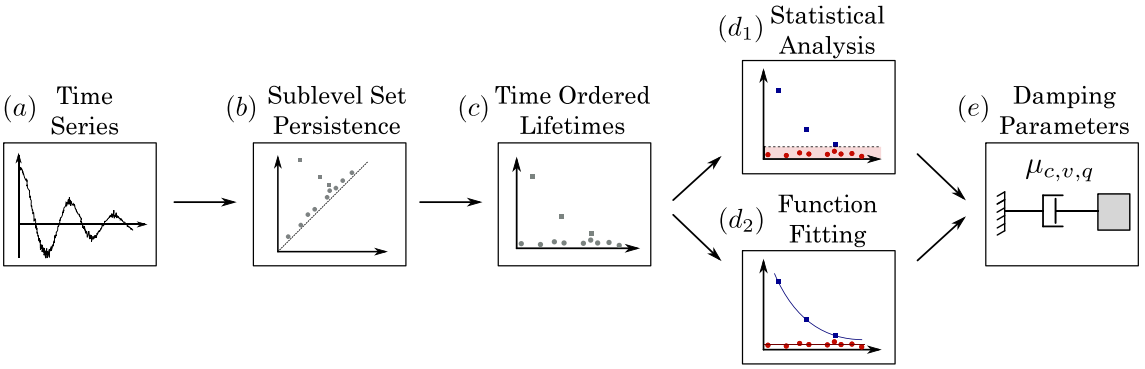

Fig. 9. Overview of method: starting with a time series, the sublevel set persistence is calculated. The lifetimes from the persistence diagram are then plotted as a function of their birth time. The resulting diagram is analyzed from both a statistical and function fitting perspective to estimate the damping parameters.

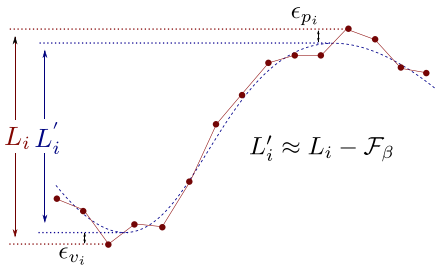

Fig. 10. Example section of sampled time series $x(t)$ with (black dots) and without (green dashed line) additive noise to demonstrate effect of additive on increasing the lifetime of sublevel set persistence by approximately $L_i - L_i' = \epsilon_{v_i} + \epsilon_{p_i} \approx \mathcal{F}_\beta$.

4.1.2. Noise floor

A secondary effect on the lifetimes associated to signal from additive noise is the increase in the lifetimes, which we term as the "noise floor" F_β. For example, consider the sample peak–valley pair shown in Fig. 10, which illustrates $x(t)$ as the original time series without noise (blue dashed line), $x(t)+\mathcal{N}$ (red dot data points), and an increase and decrease in the local maxima and minima by approximately ϵ_{p_i} and ϵ_{v_i}, respectively. Additionally, from Fig. 10, we can approximate the original noise-free lifetimes

$$L_i' \approx L_i - \epsilon_{L_i}, \tag{30}$$

where L_i is the lifetime associated to the signal with additive noise and ϵ_{L_i} is the uncertainty in the lifetime associated to signal from additive noise.

We attempt to approximate the increase in the lifetime from this uncertainty as the noise floor $F_\beta \approx \epsilon_{L_i}$. This uncertainty will generally increase the lifetime associated to signal and will consequently alter the calculations for the damping constants. Therefore, we will attempt to approximate $\mathcal{F}_\beta$ and reduce the measure lifetimes accordingly as $L_i - \mathcal{F}_\beta$.

It is straightforward to realize that ϵ_L is distributed the same as the lifetimes associated to additive noise. Therefore, our goal will be to approximate, on average, what the increase in L_i from additive noise using our previously derived statistics and resulting cutoff equations. Specifically, our goal is to represent the value of F_β as a function of the number of points near the local extrema n_e, the assumed additive noise model, and the approximate distribution parameter from the median lifetime with signal compensation (e.g. σ^* for Gaussian additive noise). To estimate F_β we will recycle the previously derived expressions from [42] in Table 1 as shown in Table 3. However, we must first develop a method to estimate n_e and an appropriate confidence level β.

We first choose an appropriate confidence level β. To determine β we consider the goal of the calculation: estimate the average increase in the lifetimes associated to signal from the additive noise near the extrema. Here, the key word is average. In comparison to the cutoff with $\alpha = 0.01$, we need a much higher confidence level for β due to our goal not being to provide a cutoff greater than the max of lifetimes associated to noise, but rather the average max itself. Therefore, we chose to set the probability as 50% or $\beta = 0.5$ such that there is an equal probability of increase in the lifetime being greater or less than the floor $\mathcal{F}_\beta$.

With β assumed as 0.5, we now need to determine n_e as the average number of points near the extrema of a lifetime associated to signal. We do not use the total number of data points n as only the points near the extrema have a significant probability of increasing L_i. Since we are working with signals of the underlying form $x(t) = A\sin(t+\phi)e(t)$ for damped oscillators with a damping envelope $e(t)$, we develop an expression for the number of samples near an extrema using the approximate response of the signal for a lifetime $L_i > C_\alpha^*$ as

$$f(x) = -\frac{L_i}{2} e(t_{B_i}) \sin(t) \tag{31}$$

Table 3
Cutoff and parameter estimation equations for the Gaussian, uniform, Rayleigh, and exponential probability distribution functions.

Distribution	Noise Floor F_β
Gaussian	$2^{3/2}\sigma^* \operatorname{erf}^{-1}\left[2(1-\sqrt{\beta})^{1/n_e}-1\right]$
Uniform	$A^*\left[2\left(1-\sqrt{\beta}\right)^{1/n_e}-1\right]$
Rayleigh	$\rho^*\left(\sqrt{-2\ln\left([1-\sqrt{\beta}]^{1/n_e}\right)}-\sqrt{-2\ln\left(1-[1-\sqrt{\beta}]^{1/n_e}\right)}\right)$
Exponential	$-\frac{1}{\lambda^*}\ln\left([1-\sqrt{\beta}]^{1/n_e}-[1-\sqrt{\beta}]^{2/n_e}\right)$

Table 4
Quick reference to equations (or cost functions) for using sublevel set persistence to estimate damping parameters and constants.

	Coulomb	Viscous	Quadratic
Parameter ζ:	$\frac{(L_i-L_{i+n})}{2(t_{B_{i+n}}-t_{B_i})}$	$\sqrt{\frac{1}{1+\left(\frac{2n\pi}{\ln(L_{i+n}/L_i)}\right)^2}}$	$C(\zeta_q)=\left[L_i-\frac{1}{2\zeta_q}\ln\left(\frac{2\zeta_q v_i-1}{2\zeta_q p_{i+1}-1}\right)\right]^2$
Constant μ:	$\frac{k(L_i-L_{i+n})}{8nN}$	$\frac{2\zeta_v k}{\omega_n}$	$C(\mu_q)=\left[L_i-\frac{m}{2\mu_q}\ln\left(\frac{2\mu_q v_i-m}{2\mu_q p_{i+1}-m}\right)\right]^2$

with the lifetime L_i born at t_{B_i} and $t\in[0,2\pi]$. We consider points near an extrema when

$$|\sin(t)|\geq 1-2\frac{C_\alpha^*}{L_i}, \tag{32}$$

where $t\in[0,2\pi]$. We now calculate the ratio between all $t\in[0,2\pi]$ and the t that satisfy Eq. (32) as

$$r_i=\frac{\{\max(t)-\min(t),\ |\sin(t)|\geq 1-2\frac{C_\alpha^*}{L_i}\}}{2\pi}, \tag{33}$$

where $r_i\in[0,1]$ and $t\in[0,2\pi]$. r_i is estimated for each L_i with the average approximated as

$$r=\text{median}(r_i). \tag{34}$$

The total number of points in the signal with the damped sinusoidal function satisfying $Ae(t)>C_\alpha^*$ is estimated as

$$N=f_s(\max(t_B)-\min(t_B)), \tag{35}$$

where f_s is the sampling frequency and t_B is the set of birth times associated to lifetimes with $L_i>C_\alpha^*$. Using the total number of points associated to signal N and the ratio of those points near the extrema, we now estimate the number of points near the extrema for a lifetime as

$$n_e=\frac{rN}{n_L}, \tag{36}$$

where n_L is the number of lifetimes with $L_i>C_\alpha^*$.

We can now implement our results for n_e, β, and the distribution parameter into the cutoff equations from Table 1 as shown in Table 3 to calculate a noise floor $\mathcal{F}_\beta$. As a note, the noise floor compensation does not have a major effect for relatively low levels of noise (e.g. SNR > 30 dB). However, for higher levels of noise the compensation can be critical for calculating an accurate estimate of the damping constant. The importance of the noise floor compensation will be shown in Section 6.

4.1.3. Damping parameter estimation

The damping parameters are estimated using the cutoff and noise floor as follows:

1. Calculate the lifetimes from the persistence diagram $L=\alpha_D-\alpha_B$ and match them with the time indices of the lifetime minima as t_B. This allows for the time ordered lifetimes plot as shown in Fig. 9.
2. With the cutoff C_α known, separate the lifetimes and birth times based on the $L>C_\alpha$. Adjust the lifetime above the cutoff using the noise floor by substituting L_i with L_i-F_β, p_i with $p_i-F_\beta/2$, and v_i with $v_i+F_\beta/2$.
3. Using the noise floor adjusted lifetimes above the cutoff and their time indices t_B, use the appropriate equation for estimating the damping constant for Coulomb, viscous, or quadratic damping (see equations referenced in Table 4). Additionally, we suggest using $i=0$ and n as the lifetime closest to $0.3211\max(L)$ to minimize the effect of additive noise as shown in [65].

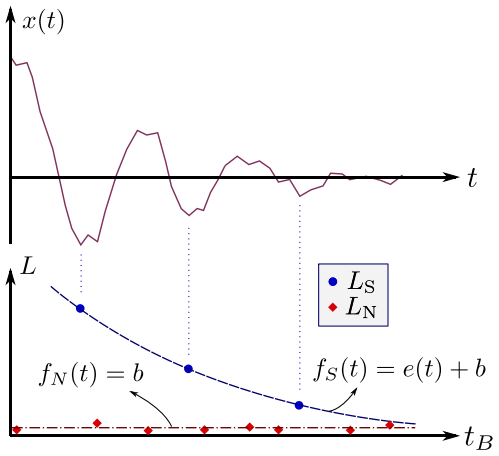

Fig. 11. Example demonstrating process of going from a time series $x(t)$ with amplitude decrement and additive noise to the time ordered lifetimes of the persistence diagram with dual function fitting.

4.2. Method 2: Function fitting to the persistence space

The second method is based on function fitting to the time ordered lifetimes. As mentioned previously, when calculating the sublevel set persistence diagram for a time series with additive noise, the persistence pairs associated to noise populate the region near the diagonal. Similarly, for the time-ordered lifetime plot the lifetimes of the persistence pairs associated to noise L_N will be near the x-axis and the lifetimes from the persistence pairs associated to signal L_S will capture the damping envelope as shown in the example signal in Fig. 11. We leverage this result as a method of filtering the noise in time series such that we can apply a function fitting to the lifetimes associated to signal.

Using all the lifetimes $L = L_N \cup L_S$, we fit two functions of the form $f_N(t) = b$ and $f_S(t) = e(t) + b$, where $e(t)$ is the envelope function for the lifetimes based on the damping type (Coulomb or viscous) with b as a constant to account for the noise offset. f_N and f_S are fit to L_N and L_S, respectively. In Fig. 11 we demonstrate this dual function fitting method. Based on this methodology, we can use the fitting parameters of $e(t)$ to determine the damping constants.

For viscous damping we estimate the envelope function as $e(t) = ae^{-ct}$, where a and c are constant parameters. The exponent parameter c correlates with Eqs. (3) and (7) with

$$\zeta_v = c/\omega_n = \frac{nc(t_{B_{i+n}} - t_{B_i})}{2\pi}. \tag{37}$$

Additionally, $\mu_v = 2mc$. For Coulomb damping we estimate the envelope function as $e(t) = -at + d$, where a is the magnitude of the slope of the linear function and d is the intercept. We use the relationship in Eq. (13) to calculate the Coulomb damping ratio as $\zeta_c = a/2$, which is extended to

$$\mu_c = \frac{\zeta_c \pi k}{2N\omega_n} = \frac{a\pi k}{4N\omega_n}. \tag{38}$$

We have now demonstrated how the function fitting method can easily be used to estimate the damping parameters from the lifetime plot (example illustrated in Fig. 11). This methods has the benefit of not needed a statistical analysis of the noise in the persistence diagram. However, the method does require an extra computational step of function fitting.

For function fitting we use a unique cost function for fitting two curves simultaneously, which is defined as

$$C = \sum_{i=0}^{T} \min\left([L_i - f_N(t_{B_i})]^2, [L_i - f_S(t_{B_i})]^2\right), \tag{39}$$

where the cost function C is a function of the parameters a, b, c for viscous damping and a, b, d for Coulomb damping. Additionally, the subscript i of L_i and t_{B_i} denote the ith sublevel set lifetime of all T lifetimes such that $i \in [1, T]$. We minimize Eq. (39) using Python's *scipy.optimize.minimize* implementation of the Broyden–Fletcher–Goldfarb–Shanno (BFGS) minimization algorithm.

A required input for the BFGS algorithm is an initial guess of the unknown parameter values. For viscous damping, we suggest the following estimations: $a = \max(L)$, $b = max(L)/100$, and $c = \ln(1/0.3299)/t_{\text{opt}}$, where t_{opt} is the birth time of the lifetime nearest to $0.3299\max(L) \neq \max(L)$. For Coulomb damping, we make the following estimations: $b = 0.1\max(L), m = \max(L)/t_opt$, and $d = \max(L)$. Through simulations we have found that these initial guesses yield accurate results for a wide range of parameter values as demonstrated in Section 6.

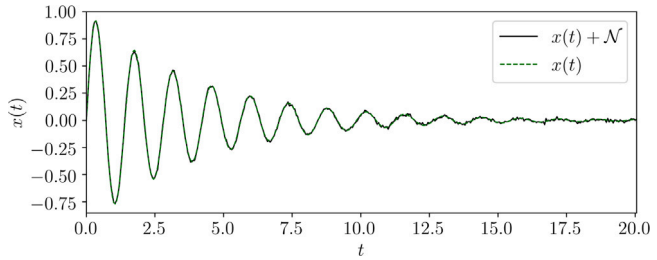

Fig. 12. Time series $x(t)$ from a viscously damped oscillator sampled at 20 Hz from Eq. (40) with and without additive noise $\mathcal{N}$ from a normal distribution with standard deviation $\sigma = 0.01$.

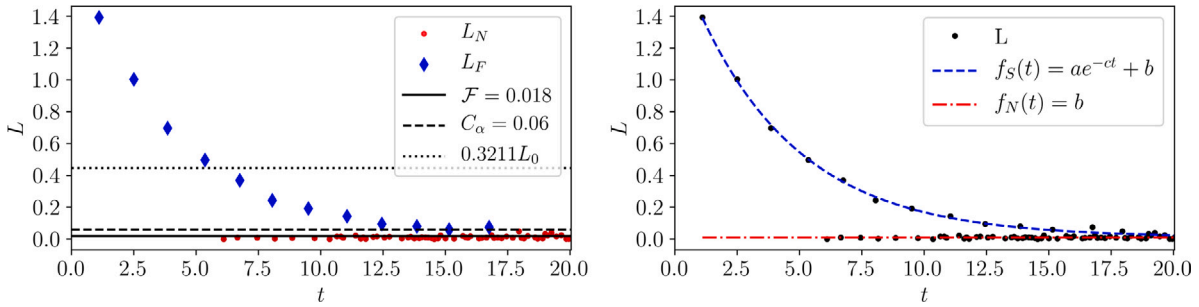

Fig. 13. Resulting time-ordered lifetimes plot for the viscous damping mechanism example in Fig. 12 with (left) the statistical analysis and (right) function fitting.

5. Examples

We now implement our method for three examples. The first example is a simulated viscously damped oscillator, the second is an experimental single pendulum with damping dominated by the Coulomb damping mechanism, and the third is a simulated quadratically damped oscillator.

5.1. Example 1: Viscously damped oscillator

For the first example, the system analyzed is the free response of the viscously damped oscillator described by $m\ddot{x} + kx + \mu_v\dot{x} = 0$, where $m = 1$ kg, $k = 20$ N/m, and $\mu_v = 0.5$ Ns/m. This system is solved as Eq. (40) with initial conditions $x_0 = 1$ m and $\dot{x}_0 = 0$ m/s as

$$x(t) = e^{-\zeta\omega_n t}\cos(\omega_d t), \tag{40}$$

where $\omega_n = \sqrt{k/m} \approx 4.472$ rad/s, $\zeta = 0.05590$, and $\omega_d = 4.465$ rad/s.

The simulation was sampled at a rate of $f_s = 20$ Hz for 20 s with additive noise $\mathcal{N}$ from a Gaussian distribution with a standard deviation $\sigma \approx 0.01$ m as shown in Fig. 12.

Sub-level set persistent homology is applied to the time series with and without additive noise as $\mathcal{P}_0(x + \mathcal{N})$ and $\mathcal{P}_0(x)$. The lifetimes L and their time indices t_B are calculated from the persistence diagram and time series, respectively. As mentioned previously, the persistence diagrams with and without additive noise show only slight differences for the significant lifetimes. We then apply both the statistics based analysis (see left side of Fig. 13) and function fitting analysis (see right side of Fig. 13) to the resulting lifetimes and time indices.

Using the lifetimes from the persistence diagram, a cutoff $C_\alpha = 0.119$ is calculated using $\alpha = 1\%$. To calculate the damping constant, the lifetime indices are chosen as $i = 0$ and $n = 3$ so that $L_{n+i}/L_i \approx 0.3211$ ($L_3/L_0 \approx 0.583/1.542 \approx 0.378$) as suggested in [65]. Using these lifetimes, ζ_v is calculated from Eq. (9) as

$$\zeta_v = \sqrt{\frac{1}{1+\left(\frac{2n\pi}{\ln(L_{i+n}/L_i)}\right)^2}} = \sqrt{\frac{1}{1+\left(\frac{6\pi}{\ln(L_3/L_0)}\right)^2}} \approx 0.05480.$$

Using ζ_v we then calculate $\mu_v = 2\zeta_v\sqrt{km} \approx 0.4901$. Both of these values are slightly below the theoretical values of $\zeta_v = 0.05590$ and $\mu_v = 0.5$. To improve the estimation, we can account for a noise floor in the calculation of ζ_v as

$$\mu_v = 2\sqrt{\frac{1}{1+\left(\frac{6\pi}{\ln(L_3-\mathcal{F}/L_0-F)}\right)^2}} \approx 0.05611,$$

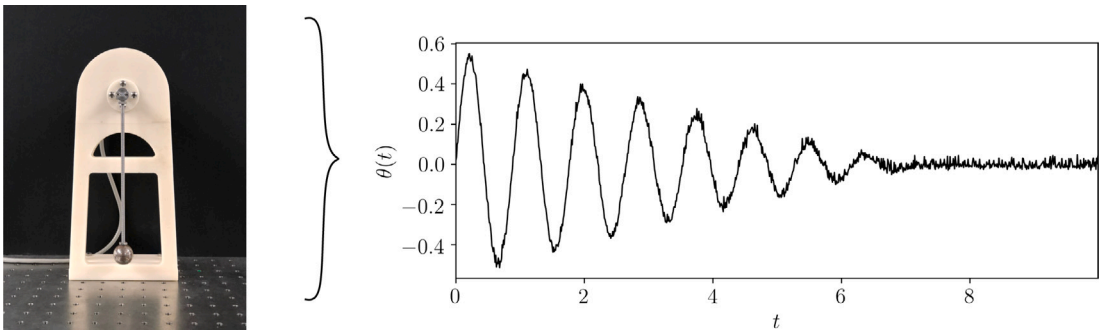

Fig. 14. Time series $x(t)$ sampled at 20 Hz from Eq. (40) with and without additive noise $\mathcal{N}$ from a normal distribution with standard deviation $\sigma = 0.01$.

where $\mathcal{F} \approx 0.018$ is calculated as described in Section 4.1.2. We calculate $\mu_v = 2\zeta_v\sqrt{km} \approx 0.5019$, which is significantly closer to the actual $\mu_v = 0.5$. This example shows that accounting for the noise floor becomes more critical as the noise level increases. We provide a thorough investigation of this in Section 6.

For the second method, we implement the dual function fitting analysis as shown on the right side of Fig. 13. This analysis results in the constant $c \approx 0.2475$, which is used in Eq. (37) to calculate $\zeta \approx 0.4955$. We then calculate $\mu_v \approx 0.05540$. This shows that the dual function fitting method also performs well for estimating the damping constants, but the statistics based method with a noise floor compensation is more accurate.

5.2. Example 2: Experimental single pendulum

The second example uses data collected from a free drop experiment of a bench top pendulum within the linear range of oscillations. The pendulum used has CAD and design documentation provided through GitHub[1] with uncertainty analysis [66]. This single pendulum has an approximate system model of the form $I\ddot{\theta} = -\mu_c \text{sgn}(\dot{\theta}) - mgr_{\text{cm}}\theta$, where $I = I_{\text{cm}} + mr_{\text{cm}}^2$ with r_{cm} as the radius to the center of mass and I_{cm} as the inertia about the center of mass. This equation can be compared to Eq. (2) with $\mu_v = \mu_q = 0$. This comparison results in equivalence of $m = I$ and $k = mgr_{\text{cm}}$.

For the pendulum model it is assumed that the other damping mechanisms are negligible in comparison to the Coulomb damping. To validate this assumption, we implemented the BFGS algorithm for fitting a simulation of the model to collected free drop data, where the three damping constants μ_c, μ_v, and μ_q were the only unknowns. This required accurate estimates for the m, r_{cm}, and I. These parameters were estimated with either a direct measurement or through SolidWorks' *mass properties* tool with an accurate CAD model, which resulted in values of $m \approx 0.1231$ kg, $I \approx 0.00295$ kg m^2, and $r_{\text{cm}} \approx 0.128$ m. From 5 free drops, our model fitting resulted in estimated average damping parameters with uncertainties (one standard deviation) of $\mu_c = (2.56 \pm 0.09) \times 10^{-3}$, $\mu_v = (1.20 \pm 0.32) \times 10^{-4}$, and $\mu_q = (6.0 \pm 2.2) \times 10^{-6}$. These parameter values show that a large majority of the damping occurred through Coulomb damping, which substantiates our reduced model for the pendulum.

If we did not have an accurate system model to estimate the damping mechanism as Coulomb, we could have validated this choice using the algorithm defined in Section 3.4. Using this algorithm we found an estimated $\omega_d = 7.14$ Rads/s and $[\zeta_c, \zeta_v, \zeta_q] = [0.0814, 0.0418, 0.1626]$ for each of the damping mechanisms. The simulated signals $\hat{\theta}(t)$ for each damping mechanism were compared to the recorded signal $\theta(t)$ using the RMSE. The resulting RMSE values for Coulomb, viscous, and quadratic damping were 0.024, 0.036, and 0.088, respectively. As such, the choice of Coulomb damping for our analysis agrees with this result. We have provided the recorded and fit signals for a qualitative analysis as shown in Fig. 15.

The collected angular data (in radians) is shown in Fig. 14. Next, similar to the first example, the time ordered lifetimes are calculated using sublevel set persistence. We can then apply both the statistics based analysis (see left side of Fig. 16) and function fitting analysis (see right side of Fig. 16) to the resulting lifetimes and time indices.

We estimate the damping parameter (slope of decrement envelope) as $\zeta_c = (L_i - L_{i+n})/2(t_{B_{i+n}} - t_{B_i})$, where $i = 0$ and $n = 5$. This calculation results in $\zeta_c \approx 0.07909$. Similarly, we use the function fitting method resulting in $a \approx 0.1538$, which is used to calculate $\zeta_c = a/2 \approx 0.07690$. Using ζ_c from the two methods, we now calculate the damping constants as $\mu_c \approx 2.65 \times 10^{-3}$ and $\mu_c \approx 2.58 \times 10^{-3}$ for the statistics and function fitting methods, respectively. Both of these results fall within the uncertainty of the parameter estimated from model fitting ($\mu_c = (2.56 \pm 0.09) \times 10^{-3}$), which suggests that this method for damping estimation is viable for experimental data.

[1] https://github.com/Khasawneh-Lab/simple_pendulum

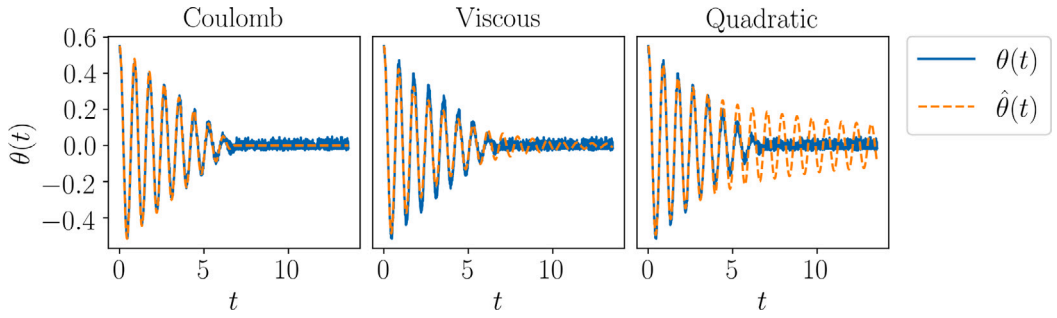

Fig. 15. Simulated signals $\hat{\theta}(t)$ for Coulomb, viscous, and quadratic damping mechanisms compared to recorded signal $\theta(t)$ with RMSE values of 0.024, 0.036, and 0.088, respectively.

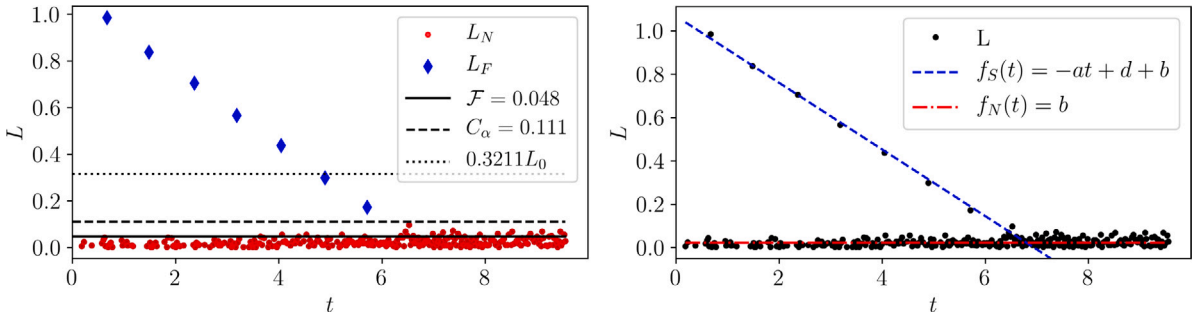

Fig. 16. Resulting time-ordered lifetimes plot for the experimental pendulum data (see Fig. 14) having an approximate Coulomb damping mechanism in the linear range with (left) the statistical analysis and (right) function fitting.

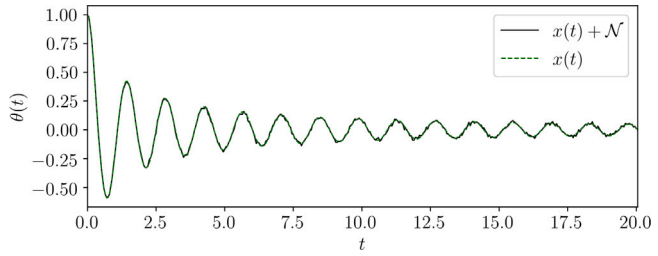

Fig. 17. Time series $x(t)$ sampled at 20 Hz from the simulation of a quadratically damped oscillator with and without additive noise $\mathcal{N}$ from a normal distribution with standard deviation $\sigma = 0.01$.

5.3. Example 3: Quadratically damped oscillator

For the last example, and completion of damping types, we again simulate a time series. However, we now use quadratic damping as the mechanism of energy dissipation. To do this, we simulate a response of

$$m\ddot{x} + kx + \mu_q \dot{x}^2 \mathrm{sgn}(\dot{x}) = 0$$

with initial conditions $x_0 = 1$ m and $\dot{x}_0 = 0$ m/s and parameters $m = 1$ kg, $k = 20$ N/m, and $\mu_q = 0.5$ Ns^2/m^2. The solution is sampled for 20 s at a sampling rate of 20 Hz. Additionally, we include additive noise $\mathcal{N}$ to the time series $x(t)$ from a Gaussian distribution with a standard deviation $\sigma \approx 0.01$ m as shown in Fig. 17.

Next, sublevel set persistence is applied to the time series with additive noise, and the corresponding birth times t_B and lifetimes L are recorded. A statistical analysis of the lifetimes is used to calculate a noise floor and cutoff as shown in Fig. 18. By minimizing the cost function in Eqs. (26) and (27), we calculate the damping constant and parameter as $\mu_q \approx 0.513$ and $\zeta_q \approx 0.513$, respectively. By comparing these values to the actual $\mu_q = 0.5$ and $\zeta_q = 0.5$, we see that sublevel set persistence is an accurate and automatic method for estimating quadratic damping parameters.

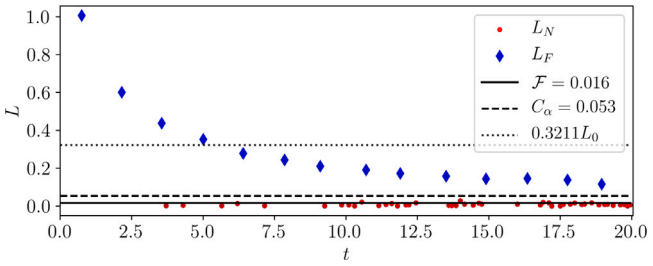

Fig. 18. Resulting time-ordered lifetimes plot for the quadratic damping mechanism example in Fig. 17 with (left) the statistical analysis and (right) function fitting.

6. Results

In this section we provide three main results of sublevel set persistence for damping parameter identification: noise robustness, functionality at low sampling frequencies, and applicability for a wide range of damping parameters. All three of these analyses are based on estimating damping parameters from the three different damping mechanisms with damping parameters of $\mu_c = 0.05$ N, $\mu_v = 0.5$ Ns/m, $\mu_q = 0.5$ Ns^2/m^2 for Coulomb, viscous, and quadratic damping, respectively. The other system parameters are set as $m = 1$ kg and $k = 20$ N/m with initial conditions $x_0 = 1$ m and $\dot{x}_0 = 0$ m/s. These systems are simulated for 20 s at a rate of 20 Hz unless specified otherwise.

6.1. Noise robustness

For analyzing noise robustness, we implement a sweep of a Signal-to-Noise-Ratio (SNR) from 15 to 40 dB, where a low SNR signifies a high level of noise. The SNR is defined as

$$\text{SNR} = 20\log_2\left(\frac{A_{\text{signal}}}{A_{\text{noise}}}\right), \tag{41}$$

where $A_{\text{signal}} = 1$ m as the maximum value of the signal (based on initial conditions), and $A_{\text{noise}} = \sigma\sqrt{2}$ with σ as the standard deviation of the additive Gaussian noise. In signal processing an SNR of 15 dB is considered the limit for extracting useful information from a time series. At each SNR, we add Gaussian (normal distribution) noise with the specified SNR and estimate the damping constant using all three methods: single lifetime, optimal lifetime ratio, and function fitting. We compute these estimates for 100 samples at each SNR, which provide a mean and standard deviation and is represented as a data point with standard deviation error bars as $\mu \pm \sigma_\mu$ (see Fig. 19). We also ran two variations of the parameter estimations: one with and one without noise compensation. By noise compensation we are referring to a compensation of the noise floor in the damping parameter estimation as described in Section 4.1.2.

Our goal with this noise robustness analysis is to determine the functional limits of each method with additive noise. On the left side of Fig. 19 we show the results with the automated noise compensation with the parameter estimation for viscous, Coulomb, and quadratic damping, from top to bottom.

For the top column of figures in Fig. 19, the results for viscous damping are shown. These results demonstrate that only the optimal noise ratio with noise compensation (left figure) accurately estimates the damping parameter ($\mu_v = 0.5$ Ns/m) at high levels of noise. At slightly lower levels of noise (SNR > 25), all three methods accurately estimate the damping parameters, but the function fitting method shows parameter estimation with higher accuracy. Similarly, for the no noise compensation case on the right, all three methods show accurate results when for SNR > 25 dB.

On the middle left figure we have the estimated Coulomb parameters (actual $\mu_c = 0.05$ N), which shows that both the function fitting and optimal ratio methods accurately estimate the damping parameter all the way down to an SNR of 15 dB. However, the damping estimation has a large uncertainty when using only a single lifetime. This suggests that the single lifetime method should only be used for low noise levels or a high SNR. Additionally, on the middle right of Fig. 19 we see almost no difference between the noise compensation and no noise compensation results suggesting that it is unnecessary to do noise compensation for Coulomb damping parameter estimation. This is most likely due to the approximately even increase in the lifetimes associated to additive noise on the lifetimes associated to signal has a minimal effect on the slope of the damping envelope.

For the last damping parameter $\mu_q = 0.5$ Ns^2/m^2 on the bottom row, there is no function fitting method as there is currently no closed-form solution for the damping envelope function for quadratic damping. This means only the single and optimal lifetime methods can be used. Additionally, for improved accuracy we see that noise compensation is necessary for SNR values less than approximately 30 dB. we also notice that quadratic damping estimation is more sensitive to additive noise than Coulomb and viscous damping and only has a relatively high precision for low noise levels with the SNR greater than approximately 30 dB.

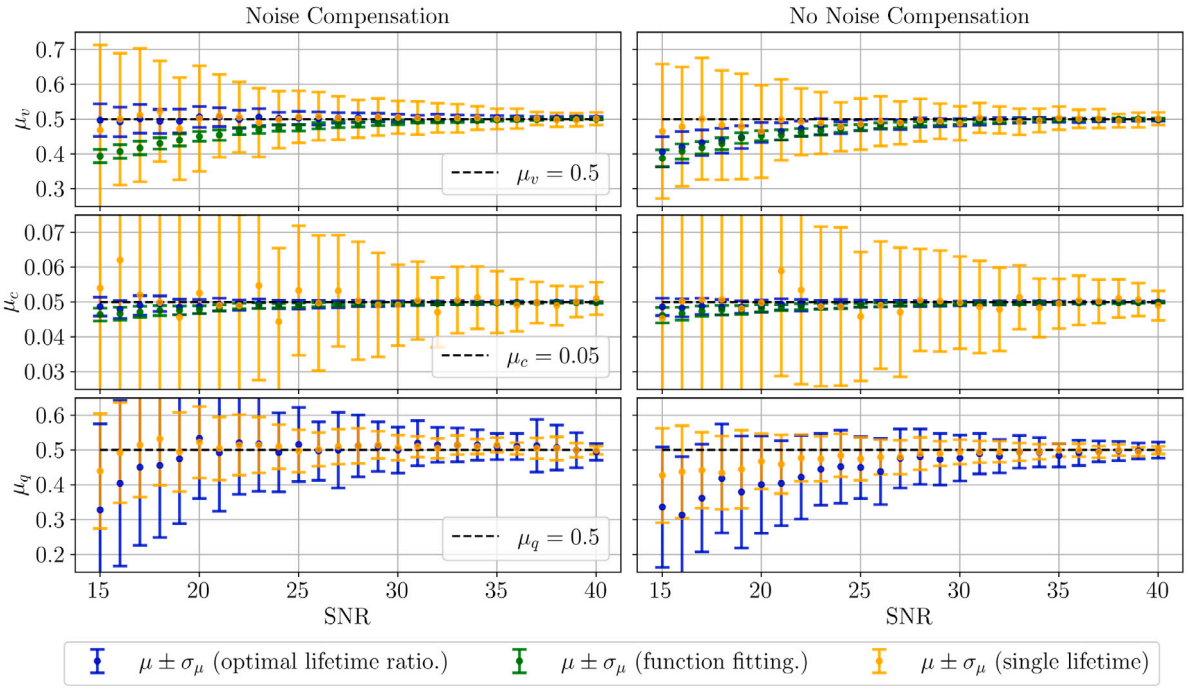

Fig. 19. Analysis of the noise robustness of sublevel set persistence for damping parameter estimation of an oscillator with (top) viscous, (middle) Coulomb, and (bottom) quadratic damping mechanisms with (left) and without (right) noise compensation. For each damping mechanism we estimate the damping parameters using a single lifetime (One), and optimal lifetime ratio (Opt.), and function fitting (Fit.).

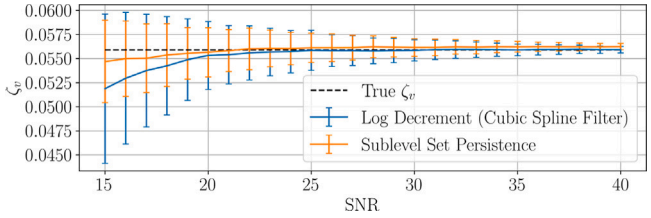

Fig. 20. Comparison between the standard logarithmic decrement method using a cubic spline filter and our sublevel set persistence method with noise compensation for estimating ζ_v with additive noise.

Comparison to a standard method. We now compare our noise compensated sublevel set persistence method to the standard logarithmic decrement method. The standard method for estimating the viscous damping ratio ζ from a signal uses the logarithmic decrement technique. However, due to additive noise in the signal a filter is needed. We chose the commonly used cubic spline filter. The cubic spline filter fits a continuous and twice differentiable piecewise cubic spline polynomial using a least squares fitting. The piecewise sections of the signal are chosen using a subset of the entire signal so that the cubic spline does not overfit to the additive noise. We use a subsampling rate such that the resulting downsampled signal has an autocorrelation intersection at $1/e$ at time delay $\tau = 3$. This downsampling rate avoids aliasing while also not overfitting to the signal. The peaks of the filtered signal are then used to estimate ζ_v using the standard log decrement technique as in Eq. (4). In Fig. 20 we make a comparison of the cubic spline logarithmic decrement method to the optimal ratio sublevel set persistence method for the viscous oscillator described in Section 5.1 with the SNR ranging from 15 to 40 dB. For each SNR 100 simulations were repeated with the mean and standard deviation as the error bars reported.

The results in Fig. 20 show that our sublevel set persistence method has less of a bias for low SNR values and is more precise than the standard log decrement method. Additionally, the log decrement method requires the additionally computational step and chosen filter parameters for filtering the signal while the sublevel set persistence method does not require any pre-processing. The cause of the bias in the log decrement method is hypothesized to stem from a distortion of the signal when applying a filter for high levels of noise.

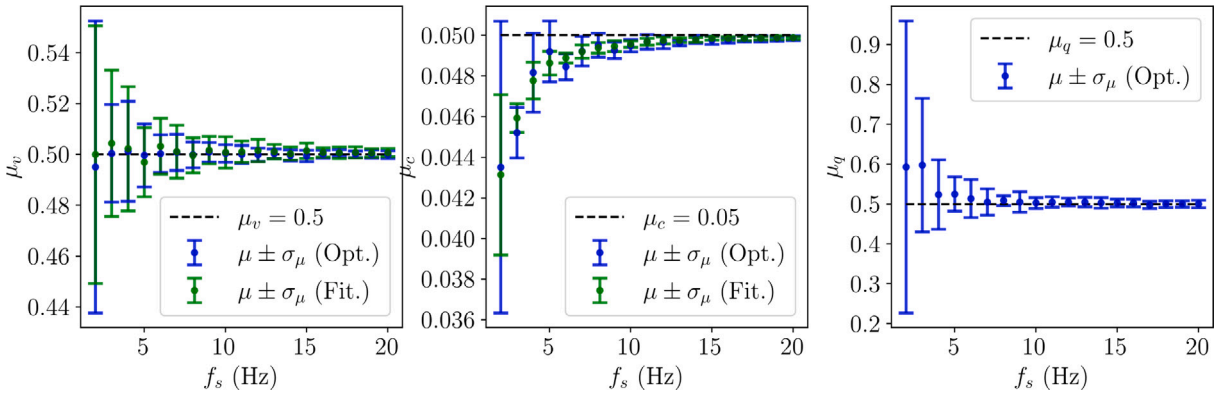

Fig. 21. Effect of low sampling frequencies for the damping parameter identification methods based on sublevel set persistence for viscous (left), Coulomb (middle), and quadratic (right) damping mechanisms. Analysis shows accurate results for sampling rate $f_s > 2f_{\text{Nyquist}}$, where $f_{\text{Nyquist}} \approx 1.42$ Hz is the Nyquist sampling rate.

6.2. Effects of sampling frequency

The second analysis of sublevel set persistence for damping parameter identification is based on the effects of sampling rate to determine the minimum sampling rate at which the method will continue to function accurately. To do this analysis we scaled the sampling frequency (originally 20 Hz) from 2 to 20 Hz. At frequencies lower than 4 Hz we are approaching the Nyquist sampling rate with $f_{\text{Nyquist}} = 2\omega_n \approx 1.42$ Hz and expect the method to fail. Additionally, we expect the accuracy will only improve for frequencies greater than 20 Hz. The additive noise level was left at 50 dB. At each frequency an uncertainty was added to the sampling frequency and the damping parameters were calculated for 100 samples. This allows for a mean and standard deviation on the parameter values (See Fig. 21).

This analysis shows that for all three damping mechanisms low sampling frequencies approaching the Nyquist sampling rate reduce the accuracy and precision of the parameter estimation. We also conclude that both the function fitting and the optimal lifetime ratio methods have similar results. However, both Coulomb and quadratic damping estimation show a significantly higher level of uncertainty for sampling rates less than 4 Hz, which suggests that the time series should be sampled at rates greater than twice the Nyquist rate. On the other hand, the viscous damping parameter estimation showed accurate results up to the Nyquist sampling rate.

6.3. Effects of damping parameter variation

The last result and analysis is the effect of damping parameters to determine at what parameters the methods fail. To do this analysis, there is no additive noise and we will only consider significantly high damping parameters as small damping should not decrease the accuracy of the optimal lifetime ratio and function fitting methods. However, at low damping parameters and high noise levels, the accuracy of the method based on the first, single lifetime will become inaccurate (we do not show this result).

For viscous damping we consider damping constants that result in damping parameters up to $\zeta_v = 1.0$ or $\mu_v \in [0.01, 8.5]$ Ns/m (i.e. critically damped). At $\zeta_v = 1.0$ the response has no oscillations, which results in no lifetimes and an upper limit for viscous damping. For Coulomb damping the range of damping constants μ_c will vary from 0.001 to 0.55 N, where at $\mu_c \approx 0.4N$ the sticking effect has a significant influence on the damping parameter estimation and causes the method to fail. Finally, for quadratic damping the damping constant does not have a large influence on the accuracy, which is why we chose a large damping constant range $\mu_q = [0.01, 8.0]$ Ns^2/m^2.

Fig. 22 shows the resulting damping constant estimates over the range of damping constants. For viscous damping on the left of Fig. 22, the function fitting method (Fit.) loses accuracy at approximately $\mu_v = 2.5$ Ns/m or $\zeta_v \approx 0.3$, the optimal lifetime ratio method loses accuracy at $\mu_v \approx 6$ Ns/m, and, finally, the method based on a single lifetime accurately estimates the damping constant almost all the way to $\zeta_v = 1.0$. For Coulomb damping both the function fitting and optimal lifetime ratio begin to lose accuracy when the number of lifetimes decreases to one. This occurs at approximately $\mu_c = 0.2$ N. Additionally, at $\mu_c \approx 0.4$ N, the sticking effect of Coulomb damping is effecting the single lifetime, which reduces the accuracy of the method based on a single lifetime. For quadratic damping on the right, the damping estimation method functions accurately for the entire damping constant range. We theorize that the function fitting method loses accuracy for high levels of damping due to a lack of data points or lifetimes associated to signal for the function to fit to. This result shows the benefit of using the statistics based method for estimating the damping ratio since it is functional for higher damping levels.

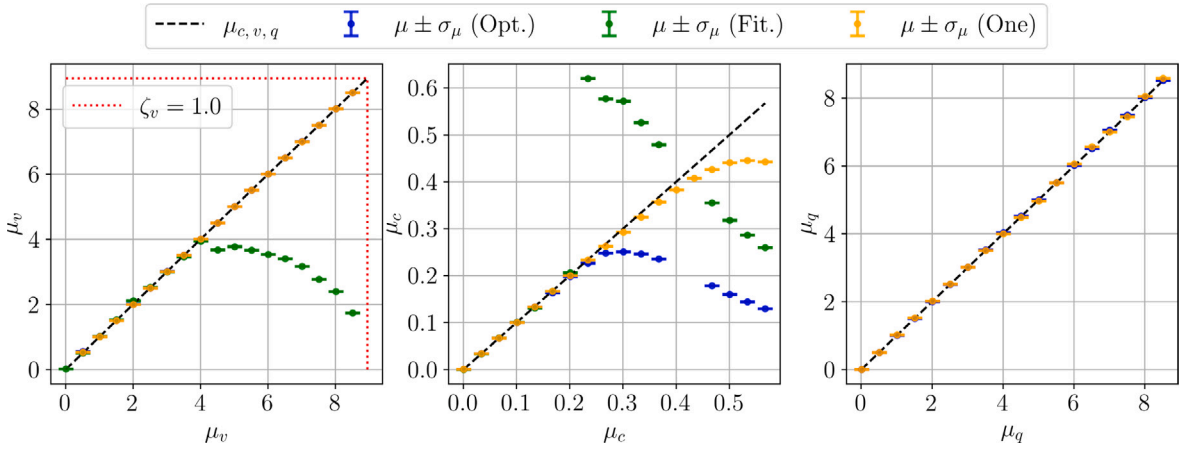

Fig. 22. Effects of damping parameters of (left) viscous, (middle) Coulomb, and (right) quadratic damping. These parameter values are ranged from very low damping to high or critical damping values.

7. Conclusion

In this work we have presented a novel time domain approach for estimating the damping parameters from the free vibration response. Specifically, we have shown how sublevel set persistence, a tool for topological data analysis, can be used to estimate viscous, Coulomb, or quadratic damping parameters. In comparison to most damping identification algorithms, we showed that this method is both computationally fast and highly automatic and only requires the time series as an input. Additionally, we showed that it is robust to a wide range of damping parameters, high levels of noise, and low sampling frequencies. Specifically, the method for estimating viscous damping is able to accurately identify the damping parameter up to critical damping ($\zeta_v = 1.0$). In addition, we applied our method to three examples exhibiting each damping mechanism with the Coulomb damping from an experimental single pendulum. We have also made the Python script implementing the methods described in this work publicly available for the easy replication of our results. Our approach is extensible to multiple degree of freedom systems, and it can be utilized for operational modal analysis by combining it, for example, with the random decrement technique. Additionally, we hypothesize that applying our method to the random decrement signature can improve damping parameter estimates due to it robustness to signal drift and additive noise in the signature. Future work involves expanding our approach to more damping models, and exploring its application to multi-degree-of freedom systems especially within operational modal analysis settings.

Declaration of competing interest

The authors declare that they have no known competing financial interests or personal relationships that could have appeared to influence the work reported in this paper.

Acknowledgment

This material is based upon work supported by the Air Force Office of Scientific Research, United States of America under award number FA9550-22-1-0007.

Appendix. Sublevel set persistence algorithm

The $O(n \log n)$ algorithm for the sublevel set persistence calculation of real-valued, one-dimensional functions is provided in Algorithm 1. This algorithm was first developed in our prior work [42] which provides more details on its implementation. We represent the time series of real numbers as an array A with length n. We begin the algorithm by creating a linked list of local extrema in A, ordered by their index in A. The begin by creating a linked list of local extrema from the array A chronologically ordered by their index which takes $O(n)$ time. We then initialize M and Q. each m in M stores the height of the extrema as $m.height$ and a pointer $m.next$ to the next element of M. The boundaries are treated as infinite classes. If the first value is a minimum we treat it as a minimum (resp., maximum) with height $-\infty$ (resp., ∞). We treat the last value similarly. We then initialize a priority queue Q to keep order of the potential minimum and maximum pairs that we could make with a priority on the smallest pairs first. q of Q stores a pair (ptr, v) with ptr as a pointer to m of M and v as the priority of $M[ptr]$. The construction of the priority queue takes $O(n \log n)$. The while loop maintains the invariant that when entering the while loop for the ith time the $i-1$ smallest persistence points have been calculated. The loop is straightforward, other than the update of Q and M. To do so, we first set $m' = m.prev$ and

remove m and $m.next$ from M as well as m', m, and $m.next$ from Q. Finally, we add m' to Q with priority $|m'.height - m'.next.height|$ The while loop executes $O(n)$ times; therefore, the total runtime of this algorithm is $O(n \log n)$.

For our specific python implementation of this algorithm, we use the *SortedList* data structure from the `Sorted Containers` Python package. Our implementation is available through the python package `teaspoon`[2].

Data: Array A of n Real Numbers
Result: Persistence Diagram
begin
  M = list of local extrema in A (non-endpoint maxima and minima);
  Q = priority queue of pointers to elements of M;
  while $|M| > 3$ **do**
    $m \leftarrow Q.pop$;
    $b \leftarrow \min\{m.height, m.next.height\}$;
    $d \leftarrow \max\{m.height, m.next.height\}$;
    Add (b, d) to *pairs*;
    Update Q and M;
  end
  return *pairs*
end

Algorithm 1: Zero-Dimensional Persistence Algorithm.

References

[1] M.S. Cao, G.G. Sha, Y.F. Gao, W. Ostachowicz, Structural damage identification using damping: a compendium of uses and features, Smart Mater. Struct. 26 (4) (2017) 043001.
[2] D. Erickson, M. Weber, I. Sharf, Contact stiffness and damping estimation for robotic systems, 2003, pp. 41–57, 22 (1).
[3] A.E.K. Mohammad, N. Uchiyama, S. Sano, Reduction of electrical energy consumed by feed-drive systems using sliding-mode control with a nonlinear sliding surface, 2014, pp. 2875–2882, 61 (6).
[4] J. Ma, Y. Sun, X. Yuan, J. Kurths, M. Zhan, Dynamics and collapse in a power system model with voltage variation: The damping effect, 2016, e0165943, 11 (11).
[5] K. Prasertwong, N. Mithulananthan, A New Algorithm Based on Logarithm Decrement to Estimate the Damping Ratio for Power System Oscillation, IEEE, 2017.
[6] R. Lin, J. Zhu, Model updating of damped structures using FRF data, Mech. Syst. Signal Process. 20 (8) (2006) 2200–2218.
[7] G. Qiao, S. Rahmatalla, Identification of damping and stiffness parameters of cervical and lumbar spines of supine humans under vertical whole-body vibration, 2019, pp. 59–71, 39 (1).
[8] A.E. Minetti, A.P. Moorhead, G. Pavei, Frictional internal work of damped limbs oscillation in human locomotion, 2020, p. 20201410, 287 (1931).
[9] T. Gupta, Identification and experimental validation of damping ratios of different human body segments through anthropometric vibratory model in standing posture, J. Biomech. Eng. 129 (4) (2006) 566–574.
[10] J.R. Moore, D.A. Maguire, Natural sway frequencies and damping ratios of trees: concepts, review and synthesis of previous studies, Trees - Struct. Funct. 18 (2) (2004) 195–203.
[11] P.M. Polunin, Y. Yang, M.I. Dykman, T.W. Kenny, S.W. Shaw, Characterization of MEMS resonator nonlinearities using the ringdown response, J. Microelectromech. Syst. 25 (2) (2016) 297–303.
[12] Y. Mo, L. Du, B. Qu, B. Peng, J. Yang, Damping ratio analysis of a silicon capacitive micromechanical accelerometer, 2017, pp. 178–188, 09 (05).
[13] T. Mimura, A. Mita, Automatic estimation of natural frequencies and damping ratios of building structures, Procedia Eng. 188 (2017) 163–169.
[14] N. Jaksic, M. Boltezar, An approach to parameter identification for a single-degree-of-freedom dynamical system based on short free acceleration response, J. Sound Vib. 250 (3) (2002) 465–483.
[15] J.W. Liang, B.F. Feeny, Identifying Coulomb and viscous friction from free-vibration decrements, Nonlinear Dynam. 16 (4) (1998) 337–347.
[16] J. H. Cole, On-The-Line Analysis of Random Vibrations, American Institute of Aeronautics and Astronautics, 1968.
[17] R.E. Aquino, Y. Tamura, Potential pitfalls in the practical application of the random decrement technique, in: Conference: 5th International Structural Specialty Conference, 2016.
[18] R. Brincker, C.E.H. Ventura, P. Andersen, Damping estimation by frequency domain decomposition, 2001.
[19] M.D.A. Hasan, Z.A.B. Ahmad, M.S. Leong, L.M. Hee, Enhanced frequency domain decomposition algorithm: a review of a recent development for unbiased damping ratio estimates, 2018, pp. 1919–1936, 20 (5).
[20] P.V. Overschee, B.D. Moor, Subspace algorithms for the stochastic identification problem, 1993, pp. 649–660, 29 (3).
[21] B. Peeters, G.D. Roeck, Reference=based stochastic subspace identification for output only modal analysis, 1999, pp. 855–878, 13 (6).
[22] G. Zhang, B. Tang, G. Tang, An improved stochastic subspace identification for operational modal analysis, 2012, pp. 1246–1256, 45 (5).
[23] U. Farooq, B. Feeny, Smooth orthogonal decomposition for modal analysis of randomly excited systems, 316 (1–5) (2008) 137–146.
[24] J.-W. Liang, B.F. Feeny, Balancing energy to estimate damping parameters in forced oscillators, J. Sound Vib. 295 (3–5) (2006) 988–998.
[25] J.-W. Liang, B.F. Feeny, Balancing energy to estimate damping in a forced oscillator with compliant contact, J. Sound Vib. 330 (9) (2011) 2049–2061.
[26] B. Mann, F. Khasawneh, An energy-balance approach for oscillator parameter identification, J. Sound Vib. 321 (1–2) (2009) 65–78.
[27] C. Meskell, A decrement method for quantifying nonlinear and linear damping parameters, J. Sound Vib. 296 (3) (2006) 643–649.
[28] F.-L. Huang, X.-M. Wang, Z.-Q. Chen, X.-H. He, Y.-Q. Ni, A new approach to identification of structural damping ratios, J. Sound Vib. 303 (1–2) (2007) 144–153.
[29] C.-S. Liu, Identifying time-dependent damping and stiffness functions by a simple and yet accurate method, J. Sound Vib. 318 (1–2) (2008) 148–165.
[30] G.A. Papagiannopoulos, G.D. Hatzigeorgiou, On the use of the half-power bandwidth method to estimate damping in building structures, Soil Dyn. Earthq. Eng. 31 (7) (2011) 1075–1079.

[2] https://lizliz.github.io/teaspoon/

[31] J. Xue, R. Diao, A frequency domain interpolation method for damping ratio estimation, in: 2014 IEEE International Conference on Control System, Computing and Engineering, ICCSCE 2014, IEEE, 2014.
[32] F. Qian, S. Leung, Y. Zhu, W. Wong, D. Pao, W. Lau, Damped sinusoidal signals parameter estimation in frequency domain, Signal Process. 92 (2) (2012) 381–391.
[33] M.R. Brake (Ed.), The mechanics of jointed structures, Springer International Publishing, 2018.
[34] M. Casiano, Extracting Damping Ratio from Dynamic Data and Numerical Solutions, Nasa Technical Reports, 2016.
[35] F.A. Khasawneh, E. Munch, Topological data analysis for true step detection in periodic piecewise constant signals, Proc. Royal Soc. A: Math. Phys. Eng. Sci. 474 (2218) (2018) 20180027.
[36] P. Lawson, A.B. Sholl, J.Q. Brown, B.T. Fasy, C. Wenk, Persistent homology for the quantitative evaluation of architectural features in prostate cancer histology, Sci. Rep. 9 (1) (2019).
[37] D. Cohen-Steiner, H. Edelsbrunner, J. Harer, Stability of persistence diagrams, Discrete Comput. Geom. 37 (1) (2006) 103–120.
[38] S. Nagarajaiah, B. Basu, Output only modal identification and structural damage detection using time frequency & wavelet techniques, Earthq. Eng. Eng. Vib. 8 (4) (2009) 583–605.
[39] C. Meskell, A decrement method for quantifying nonlinear and linear damping in multidegree of freedom systems, ISRN Mech. Eng. 2011 (2011) 1–7.
[40] J. Rodrigues, R. Brincker, Application of the random decrement technique in operational modal analysis, 2005.
[41] S.J. Elliott, M.G. Tehrani, R.S. Langley, Nonlinear damping and quasi-linear modelling, 2015, p. 20140402, 373 (2051).
[42] B.T.F. Audun D. Myers, Separating persistent homology of noise from time series data using topological signal processing, 2020, arXiv:2012.04039 [Math.AT].
[43] L. Edelsbrunner, Zomorodian, Topological persistence and simplification, Discrete Comput. Geom. 28 (4) (2002) 511–533.
[44] J.A. Perea, J. Harer, Sliding windows and persistence: An application of topological methods to signal analysis, Found. Comput. Math. (2015) 1–40.
[45] C.J. Tralie, J.A. Perea, (Quasi)periodicity quantification in video data, using topology, SIAM J. Imag. Sci. 11 (2) (2018) 1049–1077.
[46] F.A. Khasawneh, E. Munch, J.A. Perea, Chatter classification in turning using machine learning and topological data analysis, IFAC-PapersOnLine 51 (14) (2018) 195–200.
[47] A.O. Melih C. Yesilli, Topological feature vectors for chatter detection in turning processes, 2019, arXiv:1905.08671.
[48] F.A. Khasawneh, E. Munch, Utilizing topological data analysis for studying signals of time-delay systems, in: T. Insperger, T. Ersal, G. Orosz (Eds.), Time Delay Systems: Theory, Numerics, Applications, and Experiments, Springer International Publishing, Cham, 2017, pp. 93–106.
[49] A. Myers, E. Munch, F.A. Khasawneh, Persistent homology of complex networks for dynamic state detection, 2019, arXiv preprint arXiv:1904.07403.
[50] S. Gholizadeh, W. Zadrozny, A short survey of topological data analysis in time series and systems analysis, 2018, arXiv preprint arXiv:1809.10745.
[51] A. Myers, F.A. Khasawneh, On the automatic parameter selection for permutation entropy, Chaos 30 (3) (2020) 033130.
[52] H. Edelsbrunner, J. Harer, Persistent homology-a survey, Contemp. Math. 453 (2008) 257–282.
[53] E. Munch, A user's guide to topological data analysis, J. Learn. Anal. 4 (2) (2017).
[54] J.A. Perea, A brief history of persistence.
[55] H. Edelsbrunner, J. Harer, Computational Topology - An Introduction, American Mathematical Society, 2010, pp. I–XII, 1–241.
[56] R.J. Adler, O. Bobrowski, S. Weinberger, Crackle: The homology of noise, Discrete Comput. Geom. 52 (4) (2014) 680–704.
[57] P. Niyogi, S. Smale, S. Weinberger, A topological view of unsupervised learning from noisy data, 2011, pp. 646–663, 40 (3).
[58] D.J. Inman, Engineering Vibration, Pearson, 2014.
[59] T.H. Fay, Coulomb damping, Int. J. Math. Educ. Sci. Technol. 43 (7) (2012) 923–936.
[60] T.H. Fay, Quadratic damping, Int. J. Math. Educ. Sci. Technol. 43 (6) (2012) 789–803.
[61] B. Smith, The quadratically damped oscillator: A case study of a non-linear equation of motion, Amer. J. Phys. 80 (9) (2012) 816–824.
[62] F. Chazal, B.T. Fasy, F. Lecci, A. Rinaldo, A. Singh, L. Wasserman, On the bootstrap for persistence diagrams and landscapes, 2013, arXiv preprint arXiv:1311.0376.
[63] B.T. Fasy, F. Lecci, A. Rinaldo, L. Wasserman, S. Balakrishnan, A. Singh, et al., Confidence sets for persistence diagrams, Ann. Statist. 42 (6) (2014) 2301–2339.
[64] N. Atienza, R. Gonzalez-Diaz, M. Rucco, Persistent entropy for separating topological features from noise in vietoris-rips complexes, J. Intell. Inf. Syst. 52 (3) (2017) 637–655.
[65] J.A. Little, B.P. Mann, Optimizing logarithmic decrement damping estimation via uncertainty analysis, in: Special Topics in Structural Dynamics & Experimental Techniques, Vol. 5, Springer International Publishing, 2019, pp. 19–22.
[66] D. Petrushenko, F.A. Khasawneh, Uncertainty propagation of system parameters to the dynamic response: An application to a benchtop pendulum, in: Volume 4B: Dynamics, Vibration, and Control, American Society of Mechanical Engineers, 2017.